A non-canonical convergence of carbohydrate and glutamine metabolism is required after metabolic rewiring in a solid environment

Peng Wei[1], Alex J. Bott[1], Ahmad A. Cluntun[1], Jeffrey T. Morgan[1], Corey N. Cunningham[1], John C. Schell[1, 8], Yeyun Ouyang[1], Scott B. Ficarro[2, 3], Jarrod A. Marto[2, 3], Nika N. Danial[2, 4], Ralph J. DeBerardinis[5, 6], Jared Rutter[1, 7, *]

[1] Department of Biochemistry, University of Utah School of Medicine, Salt Lake City, UT 84112, USA
[2] Department of Cancer Biology, Dana-Farber Cancer Institute, Harvard Medical School, Boston, MA 02115, USA
[3] Blais Proteomics Center, Dana-Farber Cancer Institute, Harvard Medical School, Boston, MA 02215, USA
[4] Department of Cell Biology, Harvard Medical School, Boston, MA 02115, USA
[5] Children's Medical Center Research Institute, University of Texas (UT) Southwestern Medical Center, Dallas, TX 75390, USA
[6] Howard Hughes Medical Institute, UT Southwestern Medical Center, Dallas, TX 75390, USA
[7] Howard Hughes Medical Institute, University of Utah School of Medicine, Salt Lake City, UT 84112, USA
[8] Present address: Department of Medicine, Massachusetts General Hospital, Boston, MA 02114, USA
[*] Correspondence: rutter@biochem.utah.edu (J. Rutter)

HIGHLIGHTS

- Mitochondrial pyruvate supports glutaminolysis in DLBCLs by supplying pyruvate for GPT2-mediated α-KG production.
- Glutamine, but not glucose, is a major carbon source for the TCA cycle in DLBCLs.
- Citrate is minimally oxidized in the TCA cycle in DLBCLs.
- MPC depletion decreases DLBCL growth in tumor xenograft assays.
- α-KG production is important for DLBCLs proliferation in a solid ECM environment.
- The mitochondrial pyruvate carrier supports DLBCL proliferation in a solid ECM environment.

SUMMARY

The fate of pyruvate, which is modulated mitochondrial pyruvate carrier (MPC) activity, is a defining metabolic feature in many cancers. Diffuse large B-cell lymphomas (DLBCLs) are a genetically and metabolically heterogenous cancer. Although MPC expression and activity differed between DLBCL subgroups, mitochondrial pyruvate oxidation was uniformly minimal. Mitochondrial pyruvate was instead robustly consumed by glutamate pyruvate transaminase 2 to support α-ketoglutarate production as part of glutamine catabolism. This led us to discover that glutamine exceeds pyruvate as a carbon source for the TCA cycle, but, MPC function is required to enable GPT2-mediated glutamine catabolism. Furthermore, we found that MPC inhibition only decreased DLBCL proliferation in a solid culture environment, but not in a suspension environment. Thus, the non-canonical connection between the consumption and assimilation of carbohydrates and glutamine in DLBCLs enables their proliferation in a solid 3D environment.

INTRODUCTION

The central pathway of carbohydrate metabolism is the conversion of glucose to pyruvate via glycolysis in the cytosol. The fate of this pyruvate is a critical metabolic node in mammalian cells. In most differentiated mammalian cells, the mitochondrial pyruvate carrier (MPC) transports pyruvate into mitochondria where it is used to fuel oxidation and anabolic reactions (Bricker et al., 2012). In contrast, in stem cells and many cancers, pyruvate is primarily converted to lactate and excreted from the cell (Vander Heiden et al., 2009), a process known as the Warburg effect. Several groups have shown in a variety of tumor types that the Warburg effect can be caused by low activity of the MPC (Schell et al., 2014; Li et al., 2017; Tang et al., 2019; Zou et al., 2019). For instance, re-expression of the MPC in colon cancer cells, which have very low native expression, increased mitochondrial pyruvate oxidation and repressed tumor growth (Schell et al., 2014). However, repression of the MPC is not a universal feature of all cancers. Indeed, in prostate cancer, high MPC activity is required for lipogenesis and oxidative phosphorylation, and, in hepatocellular carcinoma, high MPC activity is required to supply mitochondrial pyruvate for the tricarboxylic acid (TCA) cycle (Bader et al., 2019; Tompkins et al., 2019). Therefore, we lack a unified understanding of the relationship between a given cancer type and its dependence on the MPC or mitochondrial pyruvate.

Diffuse large B-cell lymphomas (DLBCLs) are the most common type of non-Hodgkin lymphoma and are genetically and phenotypically heterogeneous (Abramson and Shipp, 2005; Lenz and Staudt, 2010). This genetic heterogeneity has been captured by independent classification schemes (Alizadeh et al., 2000; Monti, 2005). In particular, consensus cluster classification has identified three subgroups of DLBCL based on gene expression and metabolic signatures: BCR-DLBCL, which are characterized by the expression of genes encoding B-cell receptor (BCR) signaling pathways; OxPhos-DLBCL, which have high expression of genes involved in mitochondrial oxidative phosphorylation; and the HR-DLBCL, which have increased expression of genes involved in host inflammatory infiltration (Monti, 2005; Caro et al., 2012; Norberg et al., 2017).

In terms of metabolism, OxPhos-DLBCLs display greater fatty acid oxidation than BCR-DLBCLs, whereas BCR-DLBCLs have a higher rate of glycolysis (Caro et al., 2012). Moreover, initial glucose tracing studies in the two subgroup suggested there might be differences in the fate of pyruvate for citrate and lactate synthesis (Caro et al., 2012). However, the qualitative and quantitative differences of carbohydrate metabolism and the broader spectrum of metabolic substrates feeding the TCA cycle, across DLBCL subgroups, including glutaminolysis and the interplay between different fuels, is not fully understood. Understanding these basic metabolism features in DLBCLs might inform their therapeutic vulnerabilities.

Although mature B cells can transition from the solid lymph node environment to the liquid intravascular environment, DLBCLs primarily form solid tumors (Bakhshi and Georgel, 2020; Chiche et al., 2019). Therefore, although DLBCLs are routinely passaged and studied in suspension media in the laboratory, mimicry of the native architecture of a solid 3D tumor microenvironment could be a key experimental factor in recapitulating DLBCL biology *ex vivo*. Therefore, we set out to examine the metabolic architectures of OxPhos-DLBCLs and BCR-DLBCLs under both suspension and Matrigel-based solid 3D growth conditions.

RESULTS

OxPhos-DLBCLs have higher MPC expression and activity than BCR-DLBCLs

OxPhos-DLBCLs exhibit elevated expression of numerous genes encoding the mitochondrial electron transport chain (ETC) subunits complexes compared to BCR-DLBCLs (Monti, 2005). Since MPC expression typically correlates with an oxidative metabolic phenotype, we hypothesized that OxPhos-DLBCLs would have higher MPC levels to compared to BCR-DLBCLs. From patient tumor microarray data (GSE10846), we found the mRNA levels of *MPC1* and *MPC2*, the genes that encode the obligatory MPC1 and MPC2 subunits of the MPC, were higher in OxPhos-DLBCL than in BCR-DLBCLs (**Fig 1A**). Across ten DLBCL cell lines, we found that OxPhos-DLBCLs generally had higher MPC1 and MPC2 protein levels than BCR-DLBCLs (**Fig 1B**). By analyzing proteomics from isolated mitochondria (Norberg et al., 2017), MPC2 was 7-fold more abundant in OxPhos-DLBCLs than BCR-DLBCLs (MPC1-derived peptides were not detected) (**Fig S1A, S1B**). MPC1 and MPC2 form an obligate heterodimer and their protein abundances are typically tightly linked, which suggests that the MPC complex is upregulated in OxPhos-DLBCLs (Schell et al., 2014).

We hypothesized that increased MPC expression in OxPhos-DLBCLs compared to BCR-DLBCLs would result in greater incorporation of carbons from glucose into the TCA cycle through increased mitochondrial transport and oxidation of pyruvate. To test this, we used D-[U-^{13}C]-glucose tracing. Surprisingly, Pfeiffer OxPhos-DLBCL cells reached only 25% incorporation of D-[U-^{13}C]-glucose into citrate within 2 hours (**Fig 1D**). MPC inhibition with UK-5099, a well-established MPC inhibitor (Halestrap, 1975), decreased glucose incorporation into citrate to 10% (**Fig 1D**). On the other hand, U2932 BCR-DLBCL cells reached a maximal incorporation of D-[U-^{13}C]-glucose into citrate of only 15% (**Fig 1D**), which was further decreased by MPC inhibition, although this change was not statistically significant (**Fig 1D**). These results indicate that the expression difference in the MPC between DLBCL subgroups is reflected in their glucose to citrate labeling, with greater glucose contribution to citrate in the OxPhos subgroup– consistent with a previous study (Caro et al 2012), but is minimal in both subgroups.

DLBCLs use mitochondrial pyruvate for GPT2-mediated alanine synthesis

Despite clearly detectable, albeit low, glucose-to-citrate labeling in DLBCL cells, we found minimal labeling of other TCA cycle intermediates, such as α-ketoglutarate (α-KG) and succinate, from D-[U-^{13}C]-glucose (**Fig 1E, 1F, 1G; Fig S1D**). This was especially evident in the BCR-DLBCL cell line, where very little α-KG and succinate labeling occurred even after four hours (**Fig 1F, 1G**). Overall, this suggests that glucose does not make a substantial contribution to the TCA cycle in DLBCLs, regardless of subtype classification. Interestingly, MPC inhibition did not increase labeling of pyruvate and lactate in either OxPhos-DLBCL or BCR-DLBCL cell lines (**Fig S1C; Fig S1D**). This is in contrast to other cell types, where inhibiting mitochondrial pyruvate import leads to an increased labeling of intracellular lactate, likely to compensate for the loss of ATP production from mitochondrial pyruvate oxidation (Cluntun et al., 2021). Altogether, these data suggest that the direct contribution of pyruvate to mitochondrial TCA cycle metabolism and ATP production is likely minimal.

Given the very limited degree to which glucose carbons were incorporated into the TCA cycle, even in OxPhos-DLBCLs that exhibit high MPC expression, we sought to uncover the destination of glucose-derived carbon once it entered the mitochondria as pyruvate. Surprisingly, we found a striking incorporation of D-[U-^{13}C]-glucose carbons into alanine. This alanine labeling was dependent on MPC activity, as MPC inhibition with UK-5099 substantially decreased labeling in both OxPhos-DLBCL and BCR-DLBCL cells (**Fig 1H; Fig S1C, S1D**). Alanine can be generated by the amination of pyruvate in either the mitochondria or cytosol. Since MPC inhibition significantly decreased the ratio of labeled alanine in DLBCLs, these data support a model wherein alanine synthesis is predominantly mediated by the mitochondrial glutamate pyruvate transaminase 2 (GPT2) enzyme, which catalyzes the reversible transamination of pyruvate and glutamate to generate alanine and α-KG (**Fig 1C**). Thus, despite

differences in MPC abundance and pyruvate oxidation in the TCA cycle, alanine is a major fate of glucose carbon in both OxPhos-DLBCLs and BCR-DLBCLs.

Glutamine feeds the TCA cycle in an MPC-dependent manner

The robust glucose-to-alanine labeling implies that substantial amounts of glutamine would need to be converted to mitochondrial glutamate for use by GPT2. The GPT2 reaction and accompanying glutamate conversion to α-KG is dependent on mitochondrial pyruvate and therefore is likely dependent upon MPC activity. Therefore, we next tested how MPC inhibition affects glutamine consumption by DLBCLs. First, we grew DLBCLs under UK-5099 treatment for five days at a series of glutamine concentrations. Neither OxPhos-DLBCL nor BCR-DLBCL cells exhibited decreased proliferation when MPC is inhibited in lower glutamine concentration media (**Fig 2A**), which suggests that MPC inhibition does not induce increased glutamine consumption or dependence in DLBCLs. This is in contrast with the metabolic responses of glioma cells, cortical neurons, and prostate cancer cells, where MPC inhibition induced increased glutamine consumption (Bader et al., 2019; Divakaruni et al., 2017; Yang et al., 2014).

To directly test if glutaminolysis is important for DLBCL growth, we inhibited the conversion of glutamine to glutamate using the well-established glutaminase (GLS1) inhibitor CB-839 (Gross et al., 2014). Treatment with CB-839 decreased proliferation in both OxPhos and BCR-BLBCL cells (**Fig 2B; Fig S2A**). Furthermore, adding a cell-permeable form of α-KG, dimethyl-α-ketoglutarate (dmKG), to DLBCLs rescued the effects of CB-839 (**Fig 2B; S2A**). This result shows that DLBCLs require α-KG generation through glutaminolysis, regardless of their subgroup classification.

To further understand how MPC inhibition affects TCA cycle metabolism, we performed a L-[U-^{13}C]-glutamine isotope tracing experiment in BCR-DLBCL cells. We found that 16% of citrate exists as the M+5 isotopologue (**Fig 2D**), which was completely eliminated upon MPC inhibition (**Fig 2D**). M+5 citrate is indicative of reductive carboxylation, wherein α-KG is converted to citrate through a backwards turn of a portion of the TCA cycle (**Fig 2C-green**) and this is thought to enable the production of citrate to fuel acetyl-CoA synthesis in the cytosol (Metallo et al., 2012; Mullen et al., 2012). Since the α-KG to citrate conversion is reversible, this result suggests the enzymes that could mediate citrate oxidation, namely isocitrate dehydrogenase 2 (IDH2) and aconitase 2 (ACO2), are active in DLBCLs.

In contrast to the minimal labeling of TCA cycle intermediates from D-[U-^{13}C]-glucose, we observed substantial labeling of M+4 succinate, M+4 fumarate, M+4 malate, and M+4 citrate from L-[U-^{13}C]-glutamine (**Fig 2D; Fig S2B**). All of these intermediates are derived from the first turn of M+5 α-KG through the TCA cycle in the oxidative direction (**Fig 2C-orange**). Surprisingly, the labeling of these TCA cycle metabolites from glutamine was significantly decreased by inhibiting the MPC (**Fig 2D; Fig S2B**). Again, this is in contrast to the increased glutamine anaplerosis observed in other cells upon MPC inhibition (Bader et al., 2019; Divakaruni et al., 2017; Yang et al., 2014). As expected, labeling from L-[U-^{13}C]-glutamine of glutamate and various isotopomers of TCA cycle intermediates is increased by 2 hours, but the same patterns of labeling remain evident (**Fig 2E**). MPC inhibition decreases this L-[U-^{13}C]-glutamine labeling and the dominant isotopomers are from reductive or the first oxidative turn of the TCA cycle (**Fig 2E; Fig S2C**). These results suggest that DLBCLs have active glutaminolysis and α-KG oxidation and that MPC activity is required for these metabolic processes by enabling α-KG production.

The extensive production of alanine from glucose also suggests that alanine could play an important role in DLBCL biosynthesis processes. To address the fate of that alanine, we cultured Pfeiffer OxPhos-DLBCL cells with D-[U-^{13}C]-glucose for 4 hours and collected the media for isotope tracing analysis. We found that M+3 alanine is robustly excreted from the cell and that this is dependent on MPC activity (**Fig 2F**;

Fig S2D). This result supports the idea that α-KG is likely the important product of GPT2 and alanine is primarily a byproduct. We also observed M+3 lactate in the media, but–unlike M+3 alanine–MPC inhibition did not affect medium M+3 lactate abundance (**Fig 2F**; **Fig S2D**), similar to our previous findings for intracellular lactate labeling (**Fig S1D**).

To summarize the above findings using L-[U-^{13}C]-glutamine isotope tracing: DLBCLs have an intact and active TCA cycle, but it is primarily fed by glutamine rather than glucose. Although glucose-to-citrate labeling occurred, the glucose-derived carbon in citrate mostly did not progress through the remainder of the TCA cycle. This is likely because of citrate export to the cytosol to support biosynthesis of fatty acid and cholesterol, as well as acetylation events via acetyl-CoA synthesis (Carrer et al., 2019; Sivanand et al., 2018).

MPC inhibition reduces DLBCLs proliferation in a solid culture environment

Given that glutamine is required as a TCA cycle fuel and thus for DLBCL proliferation, and mitochondrial pyruvate is required to sustain said glutamine oxidation, we hypothesized that loss of MPC function should impair proliferation of DLBCLs. However, inhibiting the MPC in cells grown in suspension culture had no effect on their proliferation (**Fig 3A; Fig S3A**). Because DLBCLs form solid tumors (Chiche et al., 2019) and we had previously observed that MPC-dependent effects on proliferation were particularly evident in a 3D environment (Schell et al., 2014), we decided to investigate if MPC inhibition impairs DLBCL proliferation in Matrigel, an extracellular matrix (ECM) used to mimic the *in vivo* 3D environment (Benton et al., 2014). Indeed, multiple DLBCL lines treated with UK-5099 exhibited 30–70% fewer cells than their corresponding control group after cultured in growth factor reduced Matrigel for 10 days (**Fig 3B**) without a change in viability (**Fig 3C**). These results indicate that MPC inhibition decreases proliferation rate of DLBCLs grown in an ECM 3D environment.

When grown in ECM, DLBCLs form compact colonies within 4–5 days of seeding. To address whether this colony formation was necessary for the MPC-dependent decrease in proliferation, we assayed DLBCL cell concentration 24 and 48 hours after plating in ECM, and found that MPC inhibition significantly decreased the cell concentration of all four DLBCL cell lines by 24–48 hours after plating (**Fig 3D**). As before, MPC inhibition does not decrease DLBCLs viability in ECM at these time points (**Fig S3B**). These results show that growth in an ECM 3D environment is sufficient to reveal an MPC-dependent growth phenotype in DLBCLs.

Given the environment-dependent effects on proliferation of MPC inhibition, we asked whether the metabolic effects we had previously observed in UK-5099-treated suspension cells were also evident in ECM-grown cells. We performed D-[U-^{13}C]-glucose tracing experiments with cells in ECM. As in suspension culture, alanine labeling was very robust and largely MPC-dependent (**Fig 3E**). We observed minimal ^{13}C-glucose labeling of most TCA cycle intermediates, including α-KG and succinate, which was MPC-dependent (**Fig 3E; Fig S3C**). As before, MPC inhibition did not increase intracellular pyruvate and lactate labeling (**Fig S3C**). These results confirm that MPC inhibition has similar effects on glucose metabolism in DLBCLs in both suspension and ECM environments.

To test whether the proliferation of DLBCL cells is MPC-dependent *in vivo*, we generated HBL1 cell lines wherein either *MPC1* or *MPC2* was knocked down by stable shRNA expression (**Fig 3F**). As we have seen previously depletion of either subunit leads to the loss of the other (Schell et al., 2014; Bensard et al., 2020). In xenograft assays, tumors from the *MPC2*-shRNA cell line showed a statistically significant decrease in volume over time (**Fig 3G**). Tumors from the *MPC1*-shRNA cell line showed a trend toward decreased volume, but it was not statistically significant. By analyzing the tumors by western blot from

MPC1 and MPC2, we found that the *MPC2*-shRNA tumors had maintained a robust depletion of MPC1 and MPC2. On the other hand, the *MPC1*-shRNA tumors, which exhibited a modest growth defect had completely recovered MPC1 and MPC2 protein abundance, presumably due to selection of higher MPC expressing cells (**Fig 3H**). Taken together, these data suggest that MPC is indeed important for DLBCL tumor growth in vivo.

ECM environment induces DLBCL metabolic reprogramming

To understand the full metabolic impact of transitioning from suspension to a solid ECM environment, we collected U2932 BCR-DLBCL cells for steady-state metabolomic analysis after growth in either suspension or ECM environment, with or without MPC inhibition, for 4 hours, 8 hours, 12 hours, or 24 hours. Through unbiased clustering of both samples and metabolites, we found that 4 hours was sufficient to induce robust changes in the metabolic landscape of ECM-grown cells (**Fig 4A**). This change at 4 hours occurs well before we observed a significant impact of MPC inhibition, which is most apparent at the 24-hour time point (**Fig 4A**). These results indicate that the growth environment has a broad and rapid impact on DLBCL metabolism. Next, we focused on how this environmental shift affects the glutamine and TCA cycle metabolic phenotypes. We observed more glutamine and less glutamate in ECM-grown cells than in suspension-grown cells (**Fig 4B**). As for TCA-cycle metabolites, α-KG was higher in ECM relative to suspension (**Fig 4C**), but MPC inhibition did not affect α-KG abundance in either growth environment (**Fig 4C**). We observed decreased abundance of the remaining TCA cycle intermediates in ECM, especially fumarate and malate (**Fig 4C**). These changes result in an increased α-KG/citrate ratio in the ECM environment, which could further increase the reductive α-KG to citrate conversion (Fendt et al., 2013). It also has been previously reported that changing from monolayer culture to spheroid growth enhanced the reductive α-KG to citrate reaction (Jiang et al., 2016). These results together demonstrate that the ECM environment significantly impacts DLBCL TCA cycle metabolism. Furthermore, MPC inhibition consistently decreased citrate and isocitrate abundance in ECM and suspension environments (**Fig 4C**). This is likely due to a combinatorial effect of decreased mitochondrial pyruvate to both limit the minimal pyruvate oxidation and to decrease α-KG generation via GPT2. We also performed a L-[U-^{13}C]-glutamine isotope tracing experiment in Pfeiffer DLBCL cells in both suspension and ECM environments. Similar to the previous U2932 glutamine tracing experiments performed in a suspension environment, MPC inhibition decreased the fractional labeling of the TCA cycle intermediates citrate and malate from glutamine at 2 hours (**Fig 4D**).

DLBCLs are sensitive to ammonia in ECM

Growth in a solid ECM environment increased α-KG abundance (**Fig 4C**), so we next asked if any of the following major α-KG-producing mitochondrial enzymes are responsible for this increase. One candidate is glutamate dehydrogenase (GDH), which converts glutamate to α-KG and produces free ammonia in the process (**Fig 5A**). Therefore, excessive GDH activity could be toxic if free ammonia cannot be efficiently cleared (Eng et al., 2010; Kappler et al., 2017; Spanaki and Plaitakis, 2012). Furthermore, it has been reported that GDH could synthesize glutamate from α-KG and environmental ammonia, to both detoxify and recycle ammonia nitrogen for use in biosynthesis processes (Spinelli et al., 2017). A second enzyme is the mitochondrial aspartate aminotransferase (GOT2), which converts glutamate to α-KG through consumption of another TCA cycle intermediate, oxaloacetate, and so does not add net carbons into the TCA cycle. (**Fig 5A**). The third enzyme, GPT2, consumes glutamate and pyruvate and yields α-KG and alanine, and thus its activity is dependent upon mitochondrial pyruvate and likely MPC activity (**Fig 5A**). Accordingly, the relative contribution of each of these enzymes—GDH, GOT2, and GPT2—to α-KG production can be differentiated based on their consumption and production of specific metabolites.

To determine if GOT2 activity is increased in response to MPC inhibition, we cultured DLBCL cells in L-[alpha-^{15}N]-glutamine-containing media for 4 hours and analyzed incorporation of ^{15}N into aspartate. We found that, in both suspension and ECM environments, MPC inhibition increased labeling of M+1 aspartate (**Fig 5B**), suggesting that MPC inhibition increases GOT2 activity in both environments. Interestingly, we also found that only 42% of glutamate was labeled from L-[alpha-^{15}N]-glutamine at 4 hours (**Fig 5B**), but 75% of glutamate was labeled from L-[U-^{13}C]-glutamine in a similar timeframe (**Fig S2C**). This is likely because of robust ^{14}N-glutamate synthesis by GDH from α-KG and environmental ^{14}N-ammonia, which has been reported to occur in human breast cancer cells (Spinelli et al., 2017). Therefore, we hypothesized that this GOT2 activity change is due to increased cellular demand for α-KG, due to impaired GPT2-mediated α-KG production. In addition, this impaired α-KG production could impair GDH-mediated incorporation of free ammonia into glutamate.

Since glutamine-to-aspartate nitrogen labeling is increased upon MPC inhibition, we next questioned if the steady-state aspartate abundance is affected by MPC inhibition. We found that in a suspension environment, MPC inhibition increased aspartate abundance by 4.5-fold; while in an ECM environment, aspartate abundance was only increased by 2-fold (**Fig 5C**). Because aspartate synthesis is directly tied to GOT2-mediated α-KG production, this result suggests that GOT2-mediated α-KG production might be lower in ECM, perhaps due to decreased availability of oxaloacetate. Therefore, we next asked if glutamate synthesis via GDH is also affected in ECM. We found that the ECM environment caused glutamate abundance to decrease by 70% (**Fig 5C**). MPC inhibition decreased glutamate abundance by about 30% in the suspension environment, but glutamate abundance was not affected by MPC inhibition in ECM (**Fig 5C**). This decreased glutamate abundance from suspension to ECM raises the possibility that either the GDH-mediated α-KG and ammonia production could have increased, or GDH-mediated ammonia recycling ability could have decreased. We next asked if DLBCLs have increased ammonia sensitivity when cultured in an ECM versus in a suspension environment. In suspension conditions, we observed dose-dependent toxicity of NH_4Cl with MPC inhibition having no additional effect (**Fig 5D**). In contrast, cells cultured in ECM were hypersensitive to NH_4Cl, and MPC inhibition caused an even further sensitization (**Fig 5E**). These data support two interesting conclusions: first, DLBCLs in ECM are more sensitive to ammonia than in suspension; and second, MPC inhibition increases ammonia sensitivity in ECM-cultured DLBCLs.

BCAA degradation is downregulated in MPC-inhibited DLBCLs

Because MPC inhibition decreased DLBCL proliferation in ECM, we next asked which metabolic pathways are affected by MPC inhibition in ECM. Through a metabolite set enrichment analysis on our steady-state metabolomics data, we found that after 12 or 24 hours of MPC inhibition in ECM, the most affected metabolite sets were those related to branched-chain amino acid (BCAA) degradation pathways (**Fig 6A; Fig S4A**). BCAA degradation includes the transamination of BCAAs such as valine, leucine, and isoleucine into their branched-chain keto acids (BCKA) i.e. alpha-ketoisovalerate (KIV), ketoisocaproate (KIC), and alpha-keto-beta-methylvalerate (KMV). In these transamination reactions, α-KG is aminated to glutamate. Therefore, our results suggest that BCAA degradation to BCKAs could be regulated by the MPC through its role in α-KG production. Although the growth environment and MPC inhibition had inconsistent effects on individual BCAAs, BCKAs were all more abundant in ECM than in suspension, and decreased by MPC inhibition (**Fig 6B**). These results suggest that MPC inhibition decreases BCKA production presumably by limiting α-KG production.

GPT2-mediated α-KG production is regulated by the MPC, and controls DLBCL proliferation

To test the hypothesis that the ECM-dependent growth defects caused by MPC inhibition were due to loss of GPT2-mediated α-KG production, we generated a *GPT2* knockdown cell line with scrambled

shRNA control (**Fig 6C**). Knockdown of *GPT2* decreased DLBCLs proliferation in ECM to a similar extent as MPC inhibition (**Fig 6C**). Importantly, we found no additive effect when the MPC was inhibited in *GPT2*-knockdown cells (**Fig 6C**). These results strongly support our model that MPC inhibition decreases DLBCL proliferation in ECM mainly by restricting mitochondrial pyruvate for the GPT2 reaction.

To confirm that our GPT2 findings were specific with MPC, we generated *GDH* knockdown cells (**Fig 6D**). GDH also produces α-KG, but does not require pyruvate for its reaction. Therefore, we expected *GDH* knockdown would have MPC-independent effects on DLBCL proliferation. As with *GPT2, GDH* knockdown decreased DLBCL proliferation in ECM to a similar extent as MPC inhibition (**Fig 6D**). However, unlike *GPT2* knockdown, MPC inhibition further suppressed proliferation of *GDH* knockdown cells (**Fig 6D**). This additive effect of MPC inhibition suggests that GDH is important for the proliferation of DLBCLs in ECM, but is likely acting through a distinct pathway from the MPC and mitochondrial pyruvate.

Finally, we added the cell-permeable form of α-KG, dmKG, to cells grown in ECM to determine if directly increasing α-KG is sufficient to rescue the effects of MPC inhibition. We found that adding dmKG alone had no effect DLBCL proliferation. Importantly, however, dmKG completely rescued the MPC inhibition-dependent proliferation defect in all of the cell lines that we tested (**Fig 6E**). This further supported the hypothesis that impaired α-KG production is the metabolic defect that underlies the MPC inhibition-induced loss of proliferation in ECM.

DISCUSSION

Based on the difference in MPC expression between OxPhos- and BCR-DLBCL subgroups, we initially set out to study potential differences in the utilization of mitochondrial pyruvate in these cell types. Indeed, OxPhos-DLBCLs display greater incorporation of pyruvate into citrate, and are more sensitive to MPC inhibition for this incorporation metric. However, although there are some differences between the two subgroups, the maximum pyruvate-to-citrate labeling ratio in both OxPhos- and BCR-DLBCL subgroups is low, and labeling of TCA-cycle metabolites downstream of citrate is almost non-existent. These findings indicate that although there are differences between OxPhos- and BCR-DLBCL pyruvate metabolism, these differences are dwarfed by the effects of a common, yet unexpected source of TCA carbon, which we discovered to be pyruvate enabled glutamine. Nevertheless, in the light of a greater understanding of the role of MPC in DLBCLs, it will be interesting to understand the differential expression of the MPC in DLBCL subtypes and whether this leads to additional phenotypes that we have yet to uncover.

Although glucose does not substantially contribute to the TCA cycle in DLBCLs, glucose-derived pyruvate does facilitate the utilization of glutamine as a TCA cycle fuel by supporting GPT2 mediated α-KG production (**Fig 7**). Glutamine tracing experiments demonstrated that glutamine-derived α-KG can be converted to citrate through either the reductive or oxidative modes of the TCA cycle (**Fig 7**). This suggests that DLBCLs have an intact and active TCA cycle, but we consistently observed limited oxidation of citrate to other TCA cycle intermediates. We speculate this is because citrate is being exported to the cytosol, where it could be used to produce acetyl-CoA for lipogenesis and acetylation, both of which are critical for cancer cells (**Fig 7**) (Carrer et al., 2019; Sivanand et al., 2018). In support of this hypothesis, the mitochondrial citrate exporter SLC25A1 appears to be essential in DLBCLs (**Fig S5A, S5B**). Therefore, DLBCLs appear to have a noncanonical TCA cycle pattern that includes export of most glucose-derived citrate to the cytosol. This is likely why glutamine, and not glucose, is so prominently incorporated into the TCA cycle in DLBCL cells: pyruvate-derived citrate is not used to fuel the TCA cycle, but glutamate-derived α-KG is.

We also speculate this previously underappreciated MPC—GPT2—α-KG axis could also play an important metabolic role outside of DLBCLs or other cancers. For example, this surprising metabolic feature of DLBCLs might be established during B-cell activation. A previous study showed that B cells increase their glucose consumption during activation, but that this increased consumption—reminiscent of our study—does not lead to labeling of TCA cycles metabolites via pyruvate (Waters et al., 2018).

Besides GPT2, GDH is another enzyme that produces α-KG from glutamate and thereby can add net carbons into the TCA cycle (**Fig 7**). Because GDH necessarily produces free ammonia while making α-KG, high GDH activity could be toxic to the cell if free ammonia does not diffuse away and cannot be efficiently recycled. Here, we show that transitioning DLBCLs from a suspension environment to a solid Matrigel-based ECM environment makes them more sensitive to ammonia. In addition, MPC inhibition further sensitizes cells to ammonia in this solid environment. We speculate that GDH-produced ammonia does not sufficiently diffuse away from cells in a solid environment, which could feed back on the GDH reaction to prevent α-KG production. As a consequence of this decreased α-KG production, less ammonia can be recycled to glutamate by GDH, resulting in a yet additional defect in the ability of the cell to detoxify excess ammonia (**Fig 7**).

A limitation of cell culture has always been an inability to fully recapitulate aspects of an individual cell's organismal context. For example, the function of pyruvate metabolism for breast cancer metastasis could only be revealed in a solid growth environment (Elia et al., 2019). The importance of this limitation varies depending on cell type. It is now clear that immune cells, including B cells, function in tissues more than in the bloodstream, as previously thought (Farber, 2021). Recent studies have reported that the tissue microenvironment could influence DLBCL gene expression (Sangaletti et al., 2020), and physical properties of the extracellular matrix environment could also change cancer cells' mitochondrial structure and function (Tharp et al., 2021). Here, we have shown that transitioning DLBCLs from a suspension environment to a solid Matrigel-based ECM rapidly reshapes their metabolome. Indeed, we found that a growth condition that better recapitulates the in vivo environment is sufficient to unveil entire facets of the DLBCL metabolic landscape not apparent in standard suspension cell culture. Indeed, we identified the environment-specific dependence on MPC activity that we then recapitulated using in vivo tumor xenograft assays. We anticipate that other aspects of DLBCL biology are also better reflected in ECM environment, and that the metabolic requirements of many types of solid-tumor cancers may be similarly revealed by more relevant culture systems.

DLBCLs are typically more vascularized compared to follicular lymphoma (Passalidou et al., 2003; Solimando et al., 2020). Aggressive and chemotherapy-resistant DLBCLs often have high vascular endothelial growth factor expression and high microvessel density (Cardesa-Salzmann et al., 2011; Ruan and Leonard, 2009; Solimando et al., 2020). Besides importing nutrients, tumor blood vessels could also function to export metabolic byproducts, such as ammonia and lactate from the tumors. In addition, cancer cells can change their metabolism to adapt to their microenvironment, such that byproducts such as ammonia and lactate become a nutrient source or anabolic substrate (Faubert et al., 2017; Spinelli et al., 2017). Since MPC inhibition affects DLBCL metabolism and induces ammonia sensitivity, it is possible that a combination therapy of an MPC inhibitor and a drug that blocks tumor blood vessel growth could sensitize cancer cells to their byproduct ammonia and also limit essential glutaminolysis.

Acknowledgements

We thank the Preclinical Research Resource, Metabolomics Core, and the Flow Cytometry Core at the University of Utah for facilitating this research, Lauren G. Zacharias and Jessica A. Sudderth in Ralph DeBerardinis's lab for their assistance with steady-state metabolism profiling and isotope tracing experiments, and members of the Rutter lab for helpful discussion. A.J.B is supported by K00CA212445. J.T.M. received support as an HHMI Fellow of the Jane Coffin Childs Memorial Fund for Medical Research. C.N.C. is supported by 1F32GM140525. N.N.D. is supported by N.I.H. grant 5R01CA219850. J.R. and R.J.D. are investigators of the Howard Hughes Medical Institute. R.J.D. is supported by N.I.H. grant R35CA22044901. The graphical abstract was created on Biorender.com with paid subscription.

Author contributions

Conceptualization, P.W., A.J.B., and J.R.; Methodology, Formal Analysis, and Investigation, P.W., A.J.B., A.A.C., J.C.S., Y.O., S.B.F., J.A.M., N.N.D., R.J.D., and J.R.; writing – original draft, P.W.; writing – review & editing, P.W., J.T.M., C.N.C., A.J.B., J.R., A.C.C., and Y.O.; Visualization, P.W., and A.J.B.; Supervision, J.R.; Funding Acquisition, J.R.

Declaration of interests

The University of Utah has filed a patent related to the mitochondrial pyruvate carrier, of which J.R. is listed as co-inventor. J.R. is a founder of Vettore Biosciences and a member of its scientific advisory board. R.J.D. is an advisor for Agios Pharmaceuticals and Vida Ventures.

REFERENCES

Abramson, J.S., and Shipp, M.A. (2005). Advances in the biology and therapy of diffuse large B-cell lymphoma: moving toward a molecularly targeted approach. Blood *106*, 1164–1174.

Alizadeh, A.A., Eisen, M.B., Davis, R.E., Ma, C., Lossos, I.S., Rosenwald, A., Boldrick, J.C., Sabet, H., Tran, T., Yu, X., et al. (2000). Distinct types of diffuse large B-cell lymphoma identified by gene expression profiling. Nature *403*, 503–511.

Bader, D.A., Hartig, S.M., Putluri, V., Foley, C., Hamilton, M.P., Smith, E.A., Saha, P.K., Panigrahi, A., Walker, C., Zong, L., et al. (2019). Mitochondrial pyruvate import is a metabolic vulnerability in androgen receptor-driven prostate cancer. Nat Metab *1*, 70–85.

Bakhshi, T.J., and Georgel, P.T. (2020). Genetic and epigenetic determinants of diffuse large B-cell lymphoma. Blood Cancer J. *10*, 123.

Bensard, C.L., Wisidagama, D.R., Olson, K.A., Berg, J.A., Krah, N.M., Schell, J.C., Nowinski, S.M., Fogarty, S., Bott, A.J., Wei, P., et al. (2020). Regulation of Tumor Initiation by the Mitochondrial Pyruvate Carrier. Cell Metabolism *31*, 284-300.e7.

Benton, G., Arnaoutova, I., George, J., Kleinman, H.K., and Koblinski, J. (2014). Matrigel: From discovery and ECM mimicry to assays and models for cancer research. Advanced Drug Delivery Reviews *79–80*, 3–18.

Bricker, D.K., Taylor, E.B., Schell, J.C., Orsak, T., Boutron, A., Chen, Y.-C., Cox, J.E., Cardon, C.M., Van Vranken, J.G., Dephoure, N., et al. (2012). A Mitochondrial Pyruvate Carrier Required for Pyruvate Uptake in Yeast, *Drosophila* , and Humans. Science *337*, 96–100.

Cardesa-Salzmann, T.M., Colomo, L., Gutierrez, G., Chan, W.C., Weisenburger, D., Climent, F., Gonzalez-Barca, E., Mercadal, S., Arenillas, L., Serrano, S., et al. (2011). High microvessel density determines a poor outcome in patients with diffuse large B-cell lymphoma treated with rituximab plus chemotherapy. Haematologica *96*, 996–1001.

Caro, P., Kishan, A.U., Norberg, E., Stanley, I.A., Chapuy, B., Ficarro, S.B., Polak, K., Tondera, D., Gounarides, J., Yin, H., et al. (2012). Metabolic Signatures Uncover Distinct Targets in Molecular Subsets of Diffuse Large B Cell Lymphoma. Cancer Cell *22*, 547–560.

Carrer, A., Trefely, S., Zhao, S., Campbell, S.L., Norgard, R.J., Schultz, K.C., Sidoli, S., Parris, J.L.D., Affronti, H.C., Sivanand, S., et al. (2019). Acetyl-CoA Metabolism Supports Multistep Pancreatic Tumorigenesis. Cancer Discov *9*, 416–435.

Chiche, J., Reverso-Meinietti, J., Mouchotte, A., Rubio-Patiño, C., Mhaidly, R., Villa, E., Bossowski, J.P., Proics, E., Grima-Reyes, M., Paquet, A., et al. (2019). GAPDH Expression Predicts the Response to R-CHOP, the Tumor Metabolic Status, and the Response of DLBCL Patients to Metabolic Inhibitors. Cell Metabolism *29*, 1243-1257.e10.

Cluntun, A.A., Badolia, R., Lettlova, S., Parnell, K.M., Shankar, T.S., Diakos, N.A., Olson, K.A., Taleb, I., Tatum, S.M., Berg, J.A., et al. (2021). The pyruvate-lactate axis modulates cardiac hypertrophy and heart failure. Cell Metabolism *33*, 629-648.e10.

Divakaruni, A.S., Wallace, M., Buren, C., Martyniuk, K., Andreyev, A.Y., Li, E., Fields, J.A., Cordes, T., Reynolds, I.J., Bloodgood, B.L., et al. (2017). Inhibition of the mitochondrial pyruvate carrier protects from excitotoxic neuronal death. Journal of Cell Biology *216*, 1091–1105.

Elia, I., Rossi, M., Stegen, S., Broekaert, D., Doglioni, G., van Gorsel, M., Boon, R., Escalona-Noguero, C., Torrekens, S., Verfaillie, C., et al. (2019). Breast cancer cells rely on environmental pyruvate to shape the metastatic niche. Nature *568*, 117–121.

Eng, C.H., Yu, K., Lucas, J., White, E., and Abraham, R.T. (2010). Ammonia Derived from Glutaminolysis Is a Diffusible Regulator of Autophagy. Science Signaling *3*, ra31–ra31.

Faubert, B., Li, K.Y., Cai, L., Hensley, C.T., Kim, J., Zacharias, L.G., Yang, C., Do, Q.N., Doucette, S., Burguete, D., et al. (2017). Lactate Metabolism in Human Lung Tumors. Cell *171*, 358-371.e9.

Fendt, S.-M., Bell, E.L., Keibler, M.A., Olenchock, B.A., Mayers, J.R., Wasylenko, T.M., Vokes, N.I., Guarente, L., Heiden, M.G.V., and Stephanopoulos, G. (2013). Reductive glutamine metabolism is a function of the α-ketoglutarate to citrate ratio in cells. Nat Commun *4*, 2236.

Gross, M.I., Demo, S.D., Dennison, J.B., Chen, L., Chernov-Rogan, T., Goyal, B., Janes, J.R., Laidig, G.J., Lewis, E.R., Li, J., et al. (2014). Antitumor Activity of the Glutaminase Inhibitor CB-839 in Triple-Negative Breast Cancer. Mol Cancer Ther *13*, 890–901.

Halestrap, A.P. (1975). The mitochondrial pyruvate carrier. Kinetics and specificity for substrates and inhibitors. Biochemical Journal *148*, 85–96.

Jiang, L., Shestov, A.A., Swain, P., Yang, C., Parker, S.J., Wang, Q.A., Terada, L.S., Adams, N.D., McCabe, M.T., Pietrak, B., et al. (2016). Reductive carboxylation supports redox homeostasis during anchorage-independent growth. Nature *532*, 255–258.

Kappler, M., Pabst, U., Rot, S., Taubert, H., Wichmann, H., Schubert, J., Bache, M., Weinholdt, C., Immel, U.-D., Grosse, I., et al. (2017). Normoxic accumulation of HIF1α is associated with glutaminolysis. Clin Oral Invest *21*, 211–224.

Lenz, G., and Staudt, L.M. (2010). Aggressive Lymphomas. N Engl J Med *362*, 1417–1429.

Li, Y., Li, X., Kan, Q., Zhang, M., Li, X., Xu, R., Wang, J., Yu, D., Goscinski, M.A., Wen, J.-G., et al. (2017). Mitochondrial pyruvate carrier function is negatively linked to Warburg phenotype *in vitro* and malignant features in esophageal squamous cell carcinomas. Oncotarget *8*, 1058–1073.

Metallo, C.M., Gameiro, P.A., Bell, E.L., Mattaini, K.R., Yang, J., Hiller, K., Jewell, C.M., Johnson, Z.R., Irvine, D.J., Guarente, L., et al. (2012). Reductive glutamine metabolism by IDH1 mediates lipogenesis under hypoxia. Nature *481*, 380–384.

Monti, S. (2005). Molecular profiling of diffuse large B-cell lymphoma identifies robust subtypes including one characterized by host inflammatory response. Blood *105*, 1851–1861.

Mullen, A.R., Wheaton, W.W., Jin, E.S., Chen, P.-H., Sullivan, L.B., Cheng, T., Yang, Y., Linehan, W.M., Chandel, N.S., and DeBerardinis, R.J. (2012). Reductive carboxylation supports growth in tumour cells with defective mitochondria. Nature *481*, 385–388.

Norberg, E., Lako, A., Chen, P.-H., Stanley, I.A., Zhou, F., Ficarro, S.B., Chapuy, B., Chen, L., Rodig, S., Shin, D., et al. (2017). Differential contribution of the mitochondrial translation pathway to the survival of diffuse large B-cell lymphoma subsets. Cell Death Differ *24*, 251–262.

Passalidou, E., Stewart, M., Trivella, M., Steers, G., Pillai, G., Dogan, A., Leigh, I., Hatton, C., Harris, A., Gatter, K., et al. (2003). Vascular patterns in reactive lymphoid tissue and in non-Hodgkin's lymphoma. Br J Cancer *88*, 553–559.

Ruan, J., and Leonard, J.P. (2009). Targeting angiogenesis: a novel, rational therapeutic approach for non-Hodgkin lymphoma. Leukemia & Lymphoma *50*, 679–681.

Schell, J.C., Olson, K.A., Jiang, L., Hawkins, A.J., Van Vranken, J.G., Xie, J., Egnatchik, R.A., Earl, E.G., DeBerardinis, R.J., and Rutter, J. (2014). A Role for the Mitochondrial Pyruvate Carrier as a Repressor of the Warburg Effect and Colon Cancer Cell Growth. Molecular Cell *56*, 400–413.

Sivanand, S., Viney, I., and Wellen, K.E. (2018). Spatiotemporal Control of Acetyl-CoA Metabolism in Chromatin Regulation. Trends in Biochemical Sciences *43*, 61–74.

Solimando, A.G., Annese, T., Tamma, R., Ingravallo, G., Maiorano, E., Vacca, A., Specchia, G., and Ribatti, D. (2020). New Insights into Diffuse Large B-Cell Lymphoma Pathobiology. Cancers *12*, 1869.

Spanaki, C., and Plaitakis, A. (2012). The Role of Glutamate Dehydrogenase in Mammalian Ammonia Metabolism. Neurotox Res *21*, 117–127.

Spinelli, J.B., Yoon, H., Ringel, A.E., Jeanfavre, S., Clish, C.B., and Haigis, M.C. (2017). Metabolic recycling of ammonia via glutamate dehydrogenase supports breast cancer biomass. Science *358*, 941–946.

Tang, X.-P., Chen, Q., Li, Y., Wang, Y., Zou, H.-B., Fu, W.-J., Niu, Q., Pan, Q.-G., Jiang, P., Xu, X.-S., et al. (2019). Mitochondrial pyruvate carrier 1 functions as a tumor suppressor and predicts the prognosis of human renal cell carcinoma. Lab Invest *99*, 191–199.

Tompkins, S.C., Sheldon, R.D., Rauckhorst, A.J., Noterman, M.F., Solst, S.R., Buchanan, J.L., Mapuskar, K.A., Pewa, A.D., Gray, L.R., Oonthonpan, L., et al. (2019). Disrupting Mitochondrial Pyruvate Uptake Directs Glutamine into the TCA Cycle away from Glutathione Synthesis and Impairs Hepatocellular Tumorigenesis. Cell Reports *28*, 2608-2619.e6.

Vander Heiden, M.G., Cantley, L.C., and Thompson, C.B. (2009). Understanding the Warburg Effect: The Metabolic Requirements of Cell Proliferation. Science *324*, 1029–1033.

Yang, C., Ko, B., Hensley, C.T., Jiang, L., Wasti, A.T., Kim, J., Sudderth, J., Calvaruso, M.A., Lumata, L., Mitsche, M., et al. (2014). Glutamine Oxidation Maintains the TCA Cycle and Cell Survival during Impaired Mitochondrial Pyruvate Transport. Molecular Cell *56*, 414–424.

Zou, H., Chen, Q., Zhang, A., Wang, S., Wu, H., Yuan, Y., Wang, S., Yu, J., Luo, M., Wen, X., et al. (2019). MPC1 deficiency accelerates lung adenocarcinoma progression through the STAT3 pathway. Cell Death Dis *10*, 148.

Wei et al., Figure 1

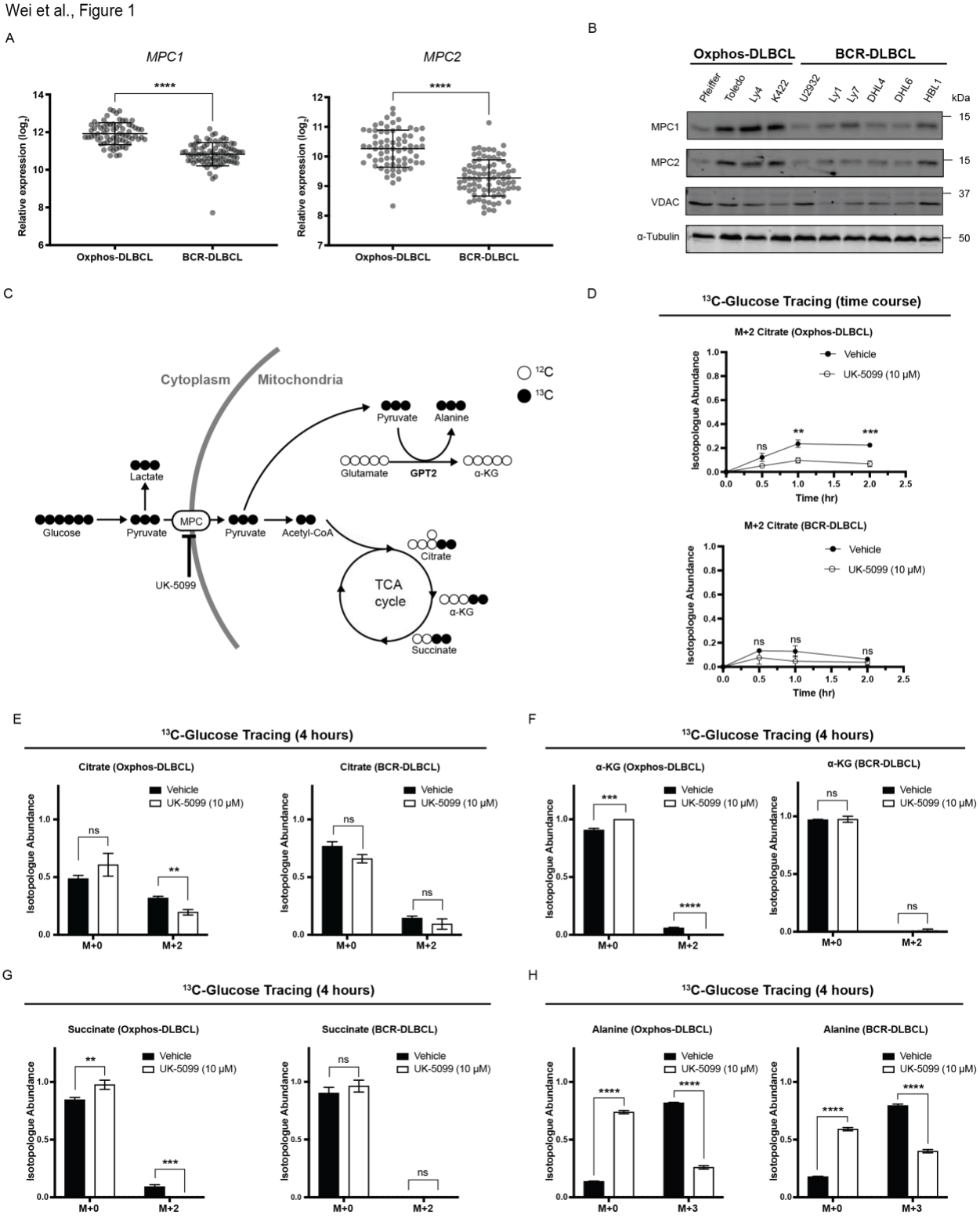

Figure 1. OxPhos- and BCR-DLBCLs have similar pyruvate metabolism profile.

(A) Aggregated MPC1 and MPC2 mRNA expression level data from 71 OxPhos- and 83 BCR-DLBCLs microarray studies.

(B) Western blot analysis of MPC1, MPC2, VDAC, and α-tubulin from a panel of OxPhos- and BCR-DLBCL cell lines.

(C) Schematic of D-[U-^{13}C]-glucose tracing.

(D) Quantification of the isotopologue abundance of M+2 citrate in OxPhos- and BCR-DLBCL cells cultured with D-[U-^{13}C]-glucose ± the MPC inhibitor UK-5099 for 30 minutes, 1 hour, and 2 hours. Isotopologue abundance is the mean of n = 3 independent biological experiments, ± standard deviation.

(E, F, G) Quantification of the isotopologue abundances of M+0 and M+2 citrate, M+0 and M+2 α-KG, and M+0 and M+2 succinate in OxPhos- and BCR-DLBCL cells cultured with D-[U-^{13}C]-glucose ± the MPC inhibitor UK-5099 for 4 hours. Isotopologue abundance is the mean of n = 3 independent biological experiments, ± standard deviation.

(H) Quantification of the isotopologue abundances of M+0 and M+3 alanine in OxPhos- and BCR-DLBCL cells cultured with D-[U-^{13}C]-glucose ± the MPC inhibitor UK-5099 for 4 hours. Isotopologue abundance is the mean of n = 3 independent biological experiments, ± standard deviation.

Vehicle: Dimethyl sulfoxide (DMSO)

ns $p > 0.05$; *$p < 0.05$; **$p < 0.01$; ***$p < 0.001$; ****$p < 0.0001$. Data were analyzed by one-way Anova followed by Dunnett's multiple comparison test.

See also Figure S1.

Wei et al., Figure 2

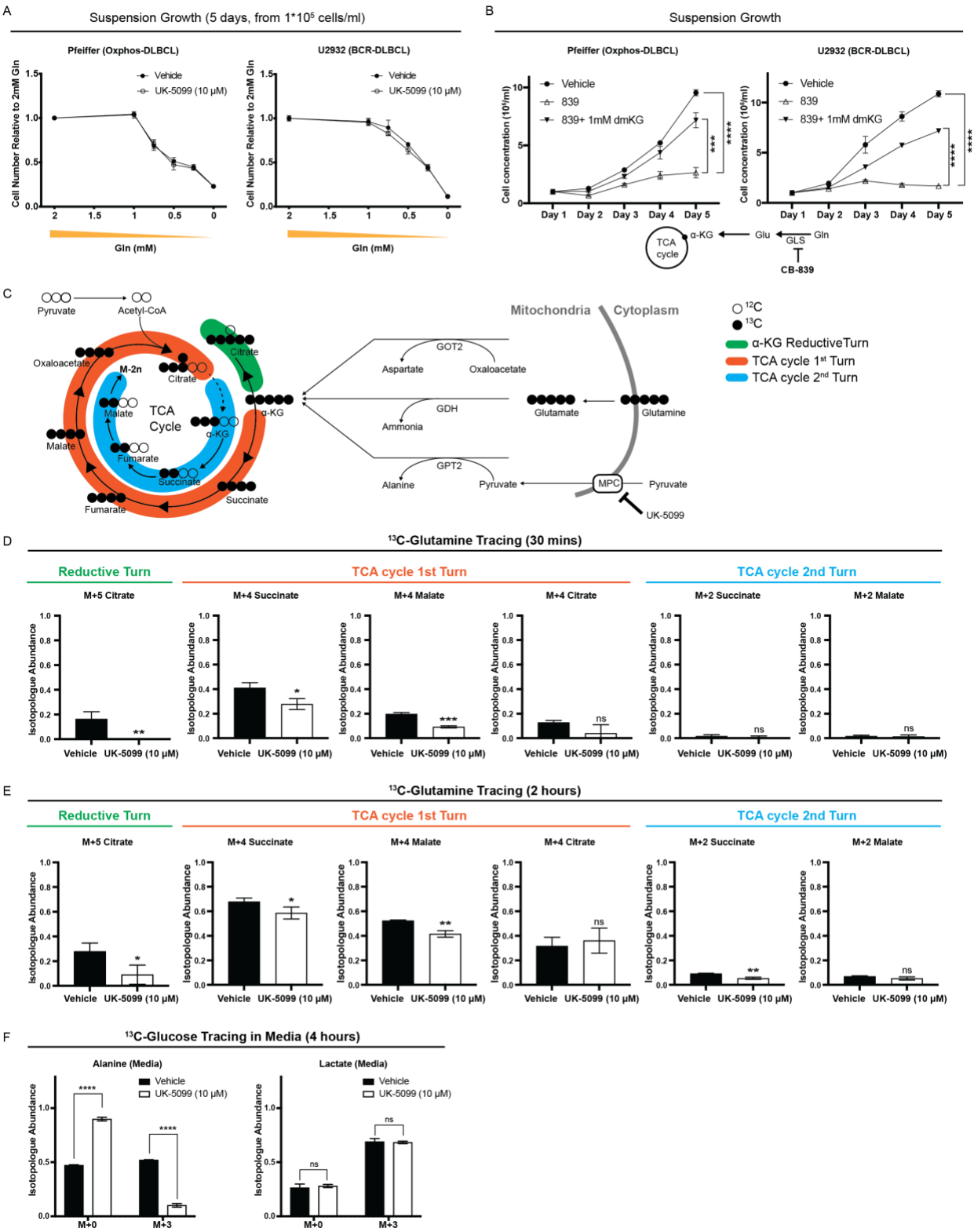

Figure 2. MPC inhibition affects glutamine to TCA cycle flux in DLBCL cells.

(A) Growth assay of OxPhos- and BCR-DLBCL cells cultured in suspension in media supplemented with 2 mM, 1 mM, 0.75 mM, 0.5 mM, 0.25 mM, or 0 mM glutamine ± the MPC inhibitor UK-5099. Cell concentration is the mean of n = 3 independent biological experiments, ± standard deviation.

(B) Growth assay of OxPhos- and BCR-DLBCL cells cultured in suspension and treated with either vehicle, GLS inhibitor CB-839, or CB-839 with dimethyl-α-ketoglutarate (dmKG). Cell concentration is the mean of n = 3 independent biological experiments, ± standard deviation.

(C) Schematic of L-[U-^{13}C]-glutamine tracing.

(D) Quantification of the isotopologue abundances of M+5 citrate, M+4 succinate, M+4 malate, M+4 citrate, M+2 succinate, and M+2 malate in DLBCL cells cultured with L-[U-^{13}C]-glutamine ± the MPC inhibitor UK-5099 for 30 minutes. Isotopologue abundance is the mean of n = 3 independent biological experiments, ± standard deviation.

(E) Quantification of the isotopologue abundances of M+5 citrate, M+4 succinate, M+4 malate, M+4 citrate, M+2 succinate, and M+2 malate in DLBCL cells cultured with L-[U-^{13}C]-glutamine ± the MPC inhibitor UK-5099 for 2 hours. Isotopologue abundance is the mean of n = 3 independent biological experiments, ± standard deviation.

(F) Quantification of the isotopologue abundances of M+0 and M+3 alanine and M+0 and M+3 lactate in the medium collected from DLBCLs grown with D-[U-^{13}C]-glucose ± the MPC inhibitor UK-5099 for 4 hours. Isotopologue abundance is the mean of n = 3 independent biological experiments, ± standard deviation.

Vehicle: Dimethyl sulfoxide (DMSO)

ns $p > 0.05$; $^{*}p < 0.05$; $^{**}p < 0.01$; $^{***}p < 0.001$; $^{****}p < 0.0001$. Data were analyzed by one-way Anova followed by Dunnett's multiple comparison test.

See also Figure S2.

Wei et al., Figure 3

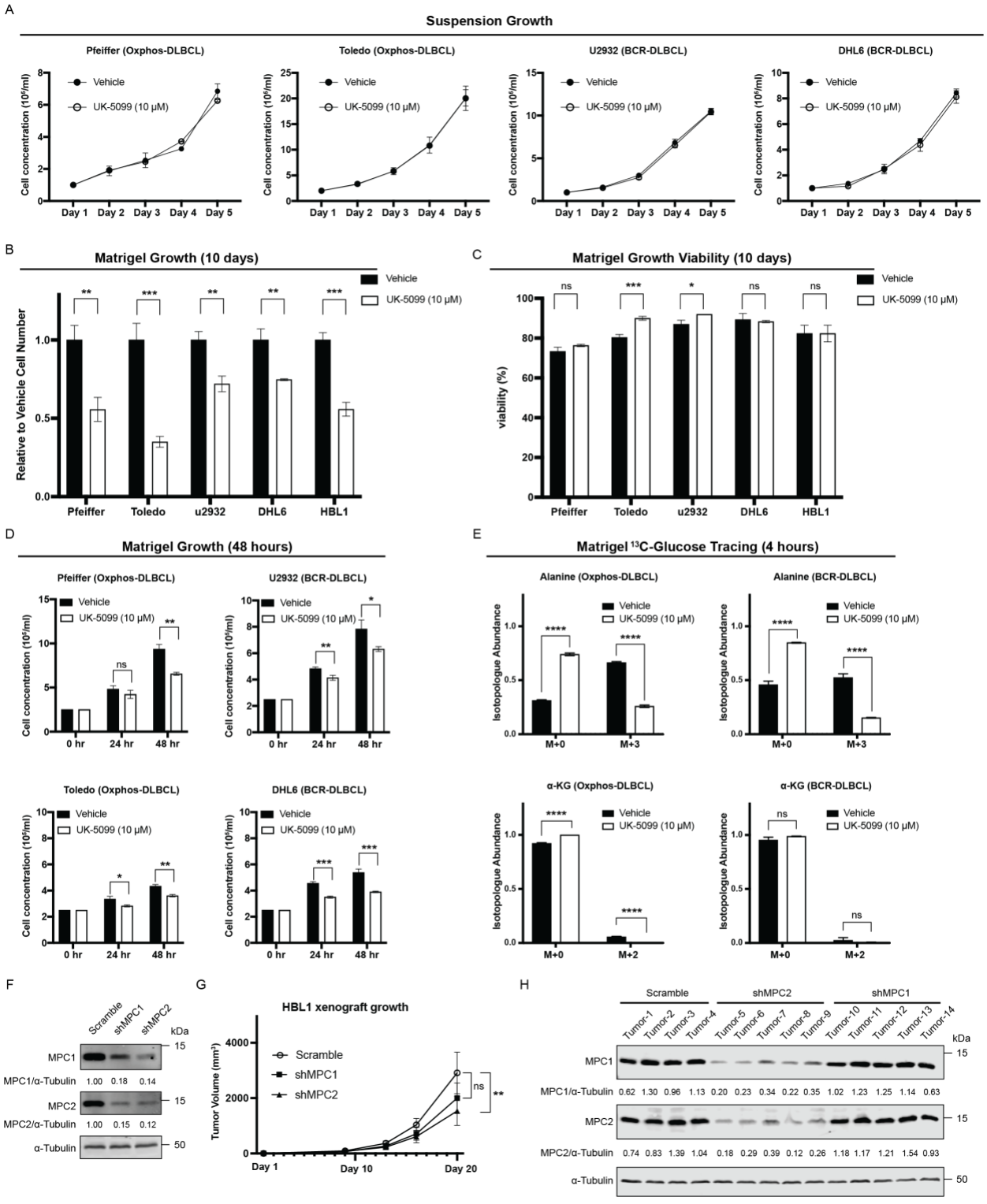

Figure 3. MPC inhibition reduces DLBCL proliferation in Matrigel.

(A) Growth assay of DLBCL cell lines cultured in suspension ± the MPC inhibitor UK-5099 for five days. Cell concentration is the mean of n = 3 independent biological experiments, ± standard deviation.

(B) Growth assay of DLBCL cell lines cultured in Matrigel ± the MPC inhibitor UK-5099 for ten days. Cell number (relative to vehicle treatment) for each cell line is the mean of n = 3 independent biological experiments, ± standard deviation.

(C) Cell viability measured by Trypan blue staining of DLBCL cell lines cultured in Matrigel ± the MPC inhibitor UK-5099 for 10 days. Cell viability is the mean of n = 3 independent biological experiments, ± standard deviation.

(D) Growth assay of DLBCL cell lines cultured in Matrigel ± the MPC inhibitor UK-5099 for 24 and 48 hours. Cell concentration is the mean of n = 3 independent biological experiments, ± standard deviation.

(E) Quantification of the isotopologue abundances of M+0 and M+3 alanine, and M+0 and M+2 α-KG from DLBCL cells cultured in Matrigel with D-[U-^{13}C]-glucose ± the MPC inhibitor UK-5099 for 4 hours. Isotopologue abundance is the mean of n = 3 independent biological experiments, ± standard deviation.

(F) Western blot analysis of MPC1, MPC2 and α-tubulin in control (Scramble) and *MPC1* or *MPC2* knock-down (shMPC1, shMPC2) HBL1 cell lines. MPC1 and MPC2 abundance was quantified and normalized to α-tubulin, with normalized abundance of the Scramble controls being set to 1.

(G) Xenograft tumor volume of control (Scramble) and *MPC1* or *MPC2* knock-down (shMPC1, shMPC2) HBL1 cell lines. Tumor volumes were determined by caliper measurement, and shown as mean of n = 4 (Scramble) or n=5 (shMPC-1 and shMPC-2) ± standard deviation.

(H) Western blot analysis of MPC1, MPC2 and α-tubulin from xenograft tumors from (G). MPC1 and MPC2 abundance was quantified and normalized to α-tubulin, with normalized abundance average of the Scramble controls being set to 1.

Vehicle: Dimethyl sulfoxide (DMSO)

ns $p > 0.05$; *$p < 0.05$; **$p < 0.01$; ***$p < 0.001$; ****$p < 0.0001$. Data were analyzed by one-way Anova followed by Dunnett's multiple comparison test.

See also Figure S3.

Wei et al., Figure 4

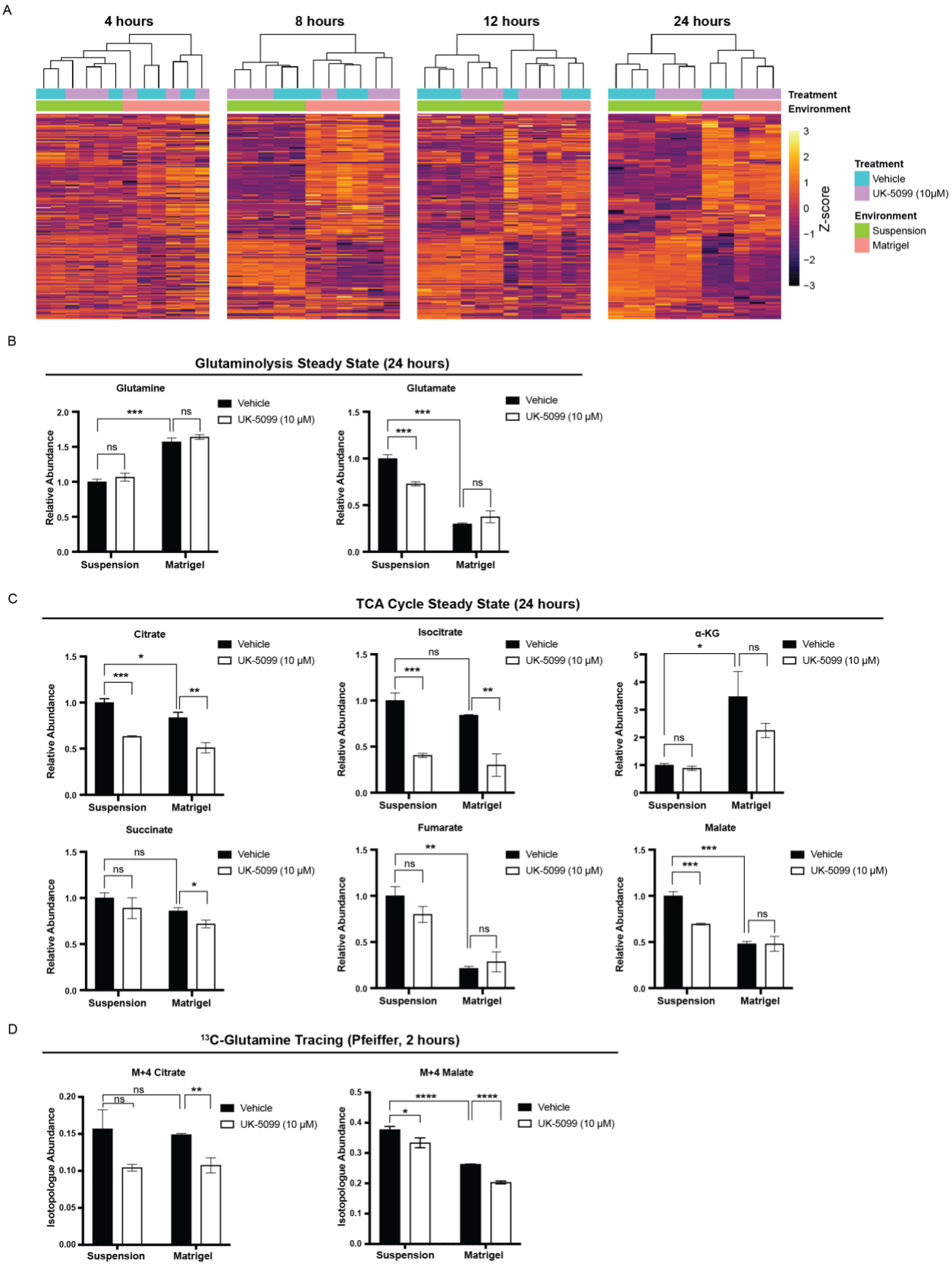

Figure 4. Environmental change reshapes the metabolic landscape of DLBCLs.

(A) Heatmaps showing the steady-state abundances of metabolites from U2932 BCR-DLBCL cells grown either in suspension or in Matrigel ± the MPC inhibitor UK-5099 for 4 hours, 8 hours, 12 hours, and 24 hours.

(B) Relative steady-state abundances of glutamine and glutamate from cells grown either in suspension or in Matrigel ± the MPC inhibitor UK-5099 for 24 hours. Metabolite abundance is the mean of n = 3 independent biological experiments, ± standard deviation.

(C) Relative steady-state abundances of citrate, isocitrate, α-KG, succinate, fumarate, and malate from cells grown either in suspension or in Matrigel ± the MPC inhibitor UK-5099 for 24 hours. Metabolite abundance is the mean of n = 3 independent biological experiments, ± standard deviation.

(D) Quantification of the isotopologue abundances of M+4 citrate and M+4 malate in Pfeiffer DLBCL cells cultured in suspension and in Matrigel with L-[U-^{13}C]-glutamine ± the MPC inhibitor UK-5099 for 2 hours. Isotopologue abundance is the mean of n = 3 independent biological experiments, ± standard deviation.

Vehicle: Dimethyl sulfoxide (DMSO)

ns $p > 0.05$; $^{*}p < 0.05$; $^{**}p < 0.01$; $^{***}p < 0.001$; $^{****}p < 0.0001$. Data were analyzed by one-way Anova followed by Dunnett's multiple comparison test.

Wei et al., Figure 5

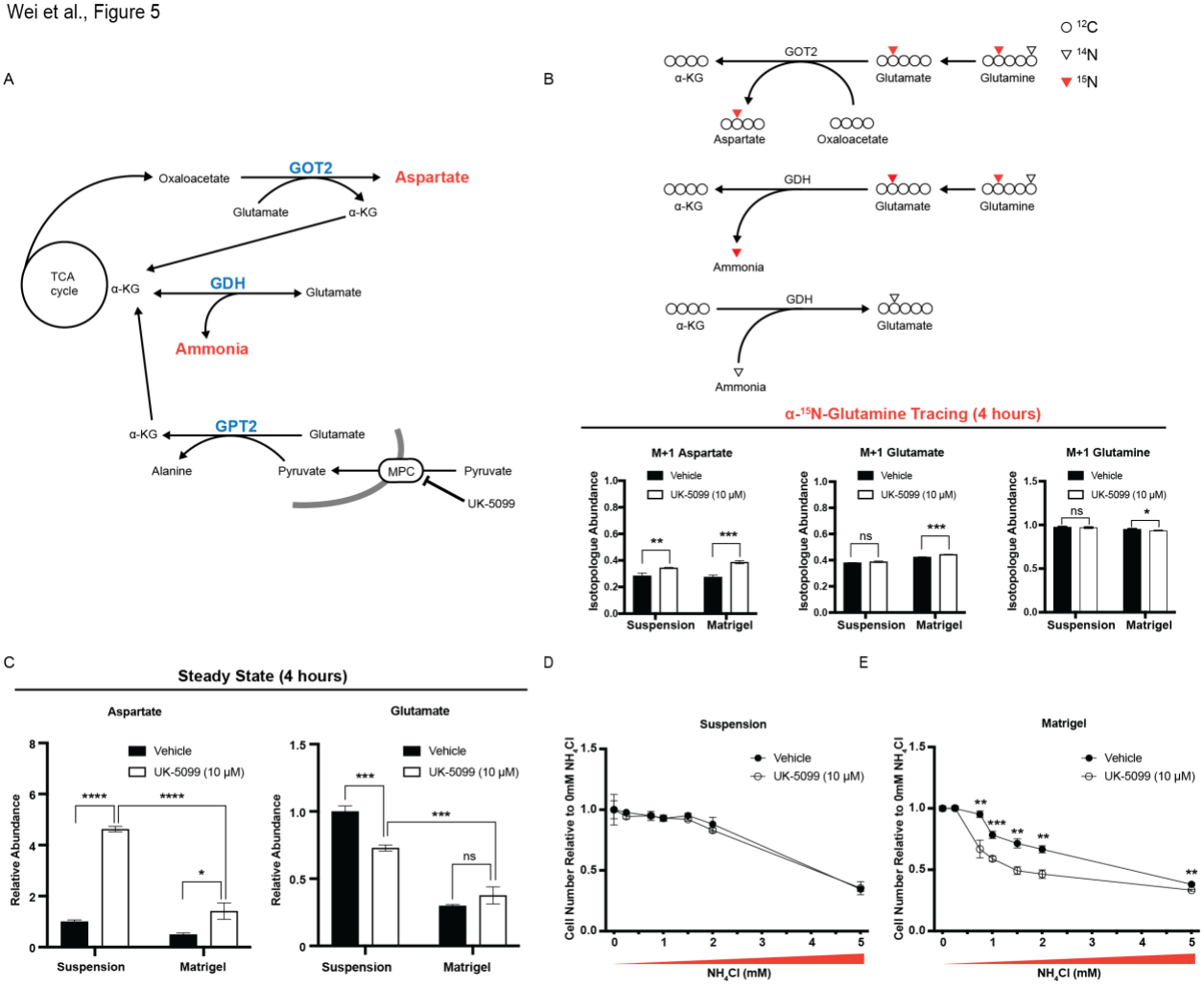

Figure 5. MPC inhibition enhances the sensitivity of DLBCLs to ammonia in Matrigel.

(A) Schematic of the metabolic interactions of α-KG production by GPT2, GOT2, and GDH with the Urea cycle.

(B) Top, schematic of L-[alpha-^{15}N]-glutamine tracing. Bottom, quantification of the isotopologue abundances of M+1 aspartate, M+1 glutamate, and M+1 glutamine in Pfeiffer DLBCL cells cultured either in suspension or in Matrigel with L-[alpha-^{15}N]-glutamine ± the MPC inhibitor UK-5099 for 4 hours. Isotopologue abundance is the mean of n = 3 independent biological experiments, ± standard deviation.

(C) Relative steady-state abundance of unlabeled (^{12}C) aspartate and glutamate from cells cultured either in suspension or in Matrigel ± the MPC inhibitor UK-5099 for 24 hours. Metabolite abundance is the mean of n = 3 independent biological experiments, ± standard deviation.

(D) Growth assay of cells cultured in suspension with 0mM, 0.3mM, 0.75mM, 1mM, 1.5mM, 2mM, and 5mM of NH_4Cl ± the MPC inhibitor UK-5099 for 48 hours. Cell number (relative to 0 mM NH_4Cl without UK-5099 treatment) is the mean of n = 3 independent biological experiments, ± standard deviation.

(E) Growth assay of cells cultured in Matrigel with 0mM, 0.3mM, 0.75mM, 1mM, 1.5mM, 2mM, and 5mM of NH_4Cl ± the MPC inhibitor UK-5099 for 48 hours. Cell number (relative to 0 mM NH_4Cl without UK-5099 treatment) is the mean of n=3 independent biological experiments, ± standard deviation.

Vehicle: Dimethyl sulfoxide (DMSO)

ns p >0.05; *p < 0.05; **p < 0.01; ***p < 0.001; ****p < 0.0001. Data were analyzed by one-way Anova followed by Dunnett's multiple comparison test.

Wei et al., Figure 6

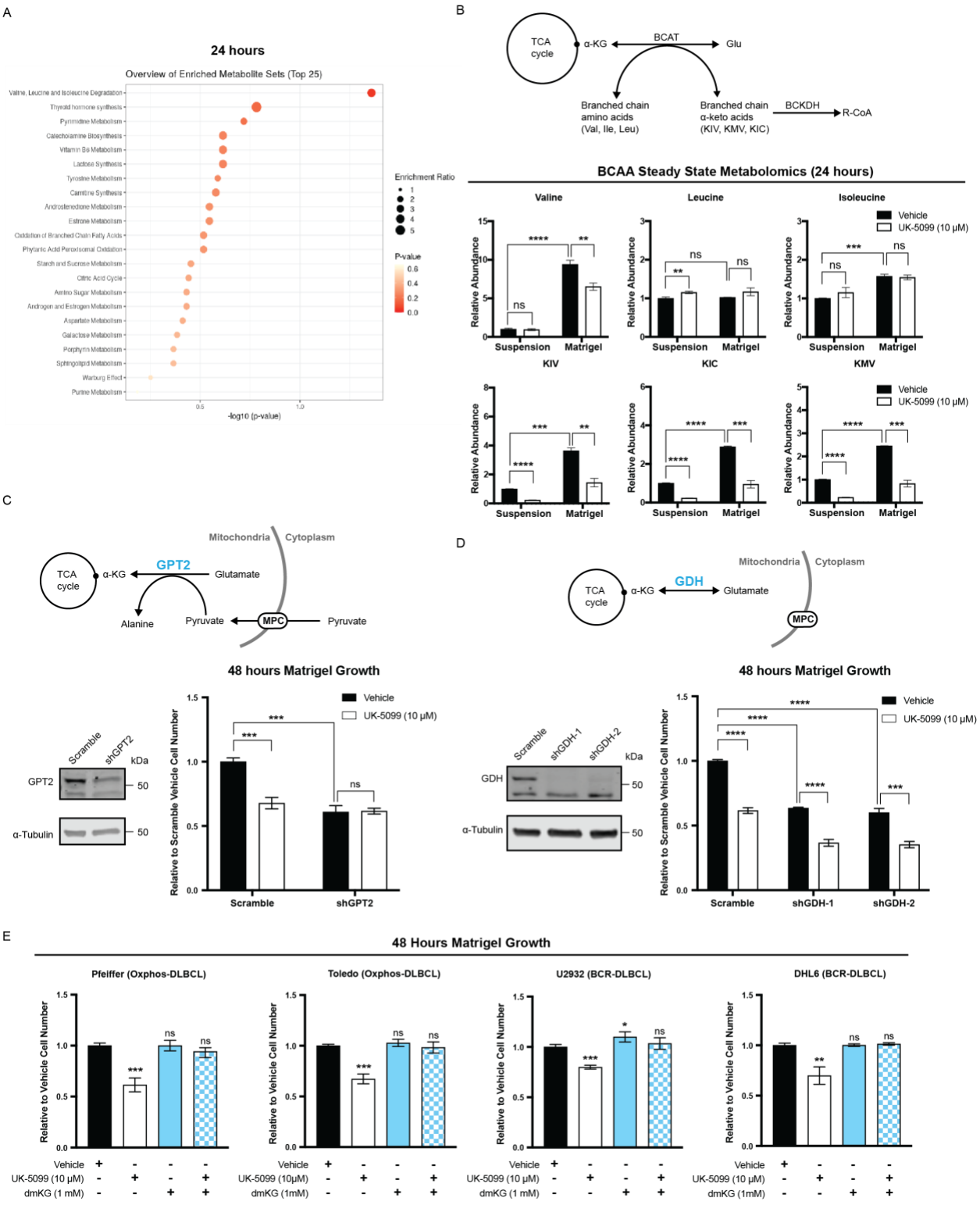

Figure 6. α-KG production supports DLBCL proliferation in Matrigel.

(A) Metabolite set enrichment analysis based on MPC inhibition (vehicle vs. UK-5099) of cells grown in Matrigel for 24 hours. Metabolite abundances are n = 3 independent biological experiments.

(B) Top, schematic of BCAA degradation pathway. Bottom, relative steady-state abundances of metabolites of the BCAA degradation pathway from cells grown either in suspension or in Matrigel ± the MPC inhibitor UK-5099 for 24 hours. Metabolite abundance is the mean of n = 3 independent biological experiments, ± standard deviation.

(C) Top, schematic of GPT2 mediated α-KG production path. Bottom left, western blot analysis of GPT2 and α-tubulin in control (Scramble) and *GPT2* knock-down (shGPT2) Pfeiffer cell lines. Bottom right, growth assay of these cell lines cultured in Matrigel ± the MPC inhibitor UK-5099 for 48 hours. Cell concentration is the mean of n = 3 independent biological experiments, ± standard deviation.

(D) Top, schematic of GDH mediated α-KG production path. Bottom left, western blot analysis of GDH and α-tubulin in control (Scramble) and *GPT2* knock-down (shGDH-1, shGDH-2) Pfeiffer cell lines. Bottom right, growth assay of these cell lines cultured in Matrigel ± the MPC inhibitor UK-5099 for 48 hours. Cell concentration is the mean of n = 3 independent biological experiments, ± standard deviation.

(E) Growth assay of cells cultured in Matrigel and treated with either vehicle, UK-5099, dimethyl-α-ketoglutarate (dmKG), or UK-5099 with dmKG for 48 hours. Cell concentration is the mean of n = 3 independent biological experiments, ± standard deviation.

Vehicle: Dimethyl sulfoxide (DMSO)

ns $p > 0.05$; $^{*}p < 0.05$; $^{**}p < 0.01$; $^{***}p < 0.001$; $^{****}p < 0.0001$. Data were analyzed by one-way Anova followed by Dunnett's multiple comparison test.

See also Figure S4.

Wei et al., Figure 7

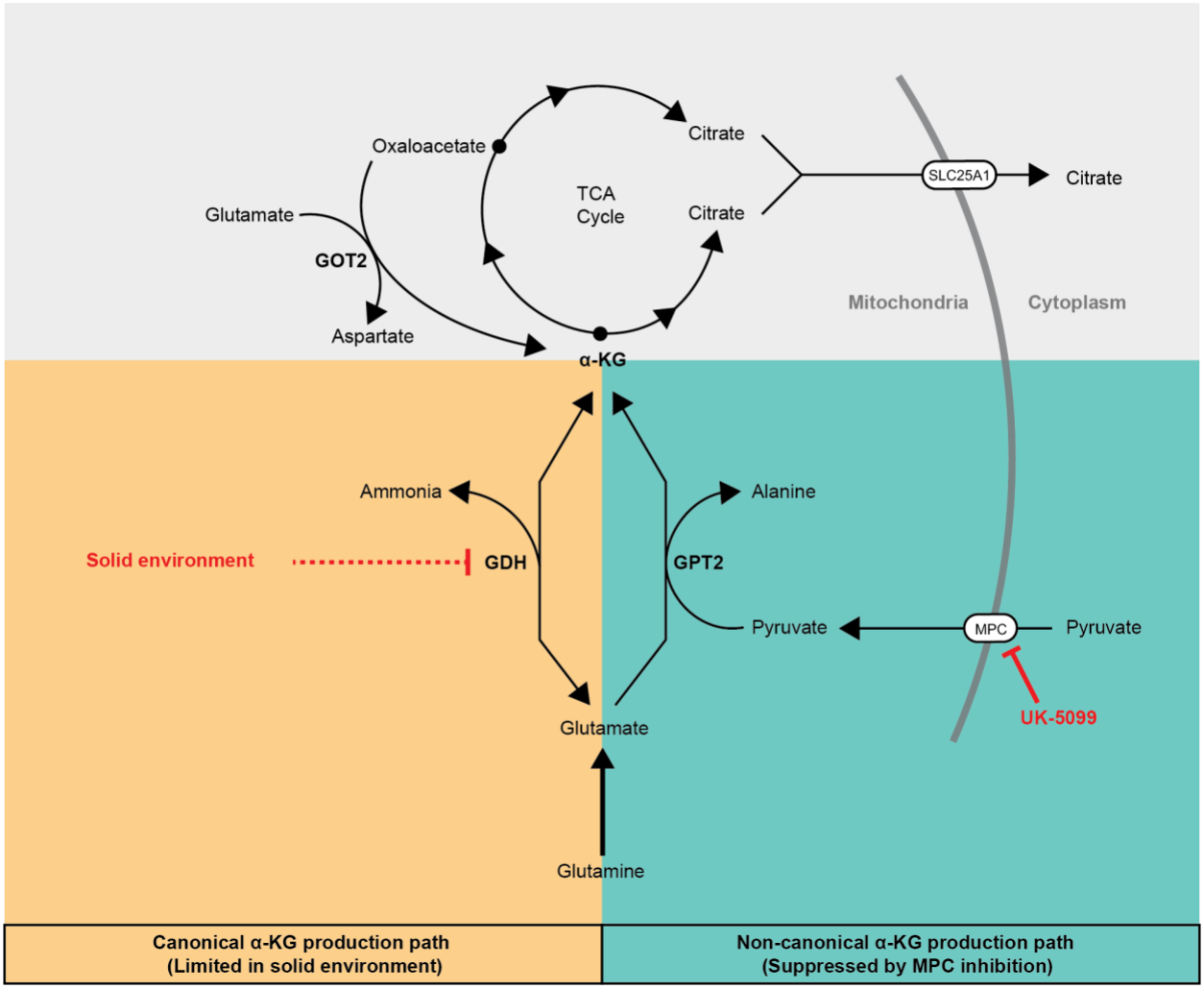

Figure 7. α-KG production paths that add net carbons to TCA cycle from glutamine.

See also Figure S5.

Wei et al., Figure S1

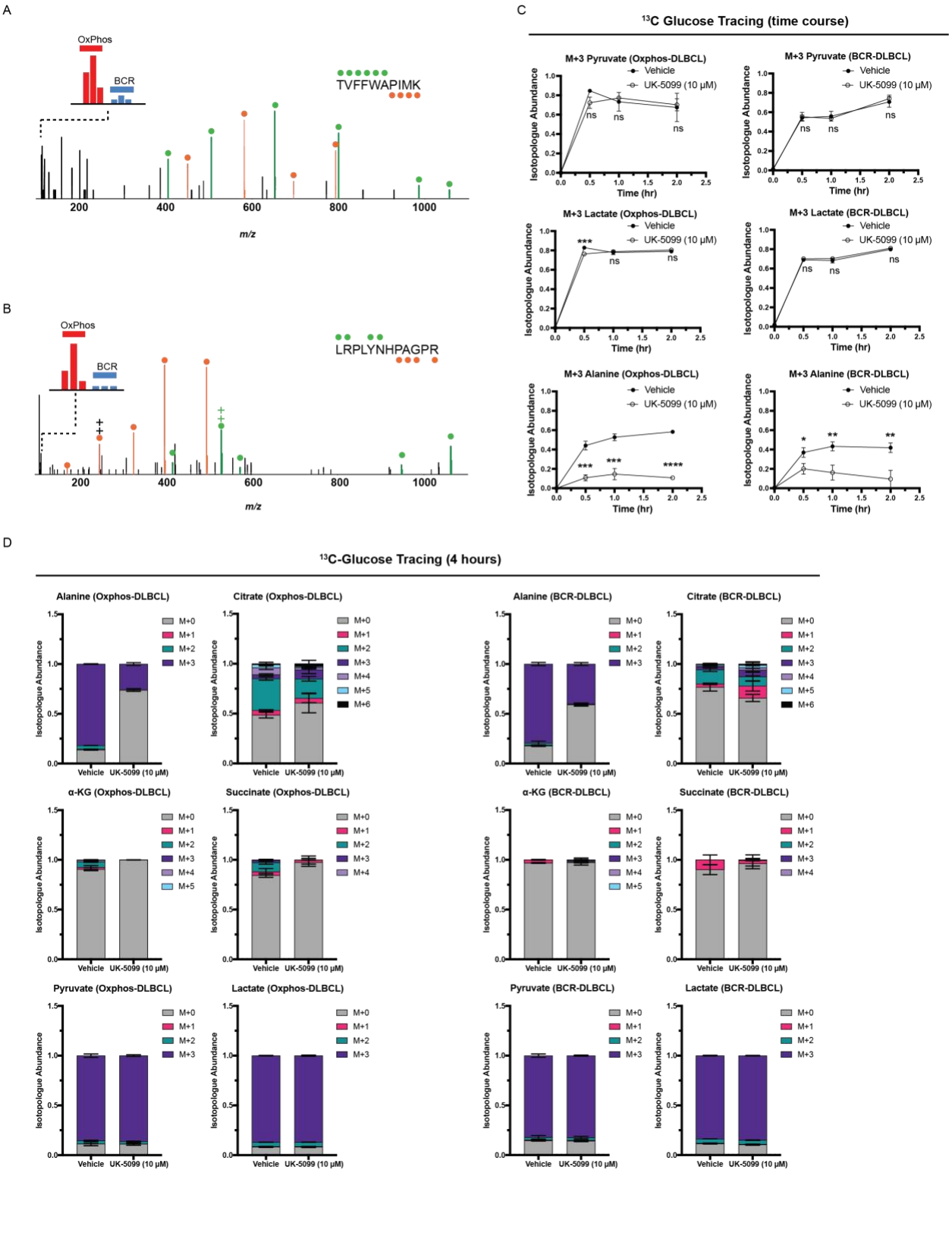

Figure S1. MPC expression and pyruvate metabolism in OxPhos- and BCR-DLBCLs. Related to Figure 1.

(A and B) MS/MS spectra corresponding to MPC2-derived peptide 40TVFFWAPIMK49 (A) and 28LRPLYNHPAGPR39 (B) acquired during multidimensional LC-MS/MS analysis of purified mitochondria from independent OxPhos- (Karpas 422, Pfeiffer, and Toledo) and three non-OxPhos/BCR- (Ly1, DHL4, and DHL6) DLBCL cell lines using DEEP SEQ mass spectrometry. Ions of b- and y-type are shown in green and orange, respectively. Relative ratios in BCR- and OxPhos-DLBCL cell lines are derived from iTRAQ reporter ion intensities shown in inset mass spectrum.

(C) Quantification of the isotopologue abundance of M+2 pyruvate, M+3 lactate, and M+3 alanine in OxPhos- and BCR-DLBCL cells cultured with D-[U-^{13}C]-glucose ± the MPC inhibitor UK-5099 for 30 minutes, 1 hour, and 2 hours. Isotopologue abundance is the mean of n = 3 independent biological experiments, ± standard deviation.

(D) Quantification of the isotopologue abundances of alanine, citrate, α-KG, succinate, pyruvate, and lactate in OxPhos- and BCR-DLBCL cells cultured with D-[U-^{13}C]-glucose ± the MPC inhibitor UK-5099 for 4 hours. Isotopologue abundance is the mean of n = 3 independent biological experiments, ± standard deviation.

Vehicle: Dimethyl sulfoxide (DMSO)

ns $p > 0.05$; *$p < 0.05$; **$p < 0.01$; ***$p < 0.001$; ****$p < 0.0001$. Data were analyzed by one-way Anova followed by Dunnett's multiple comparison test.

Wei et al., Figure S2

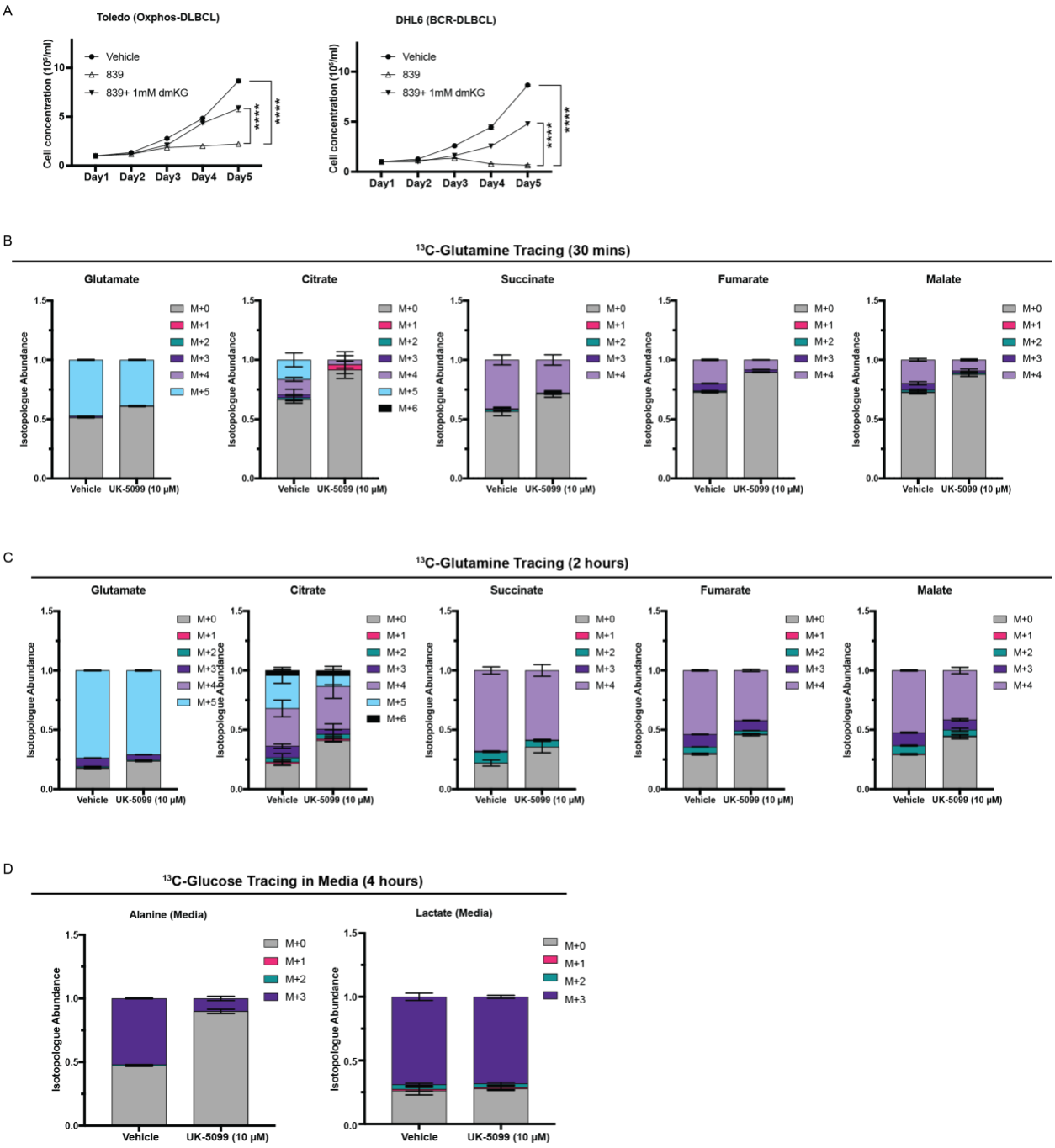

Figure S2. α-KG production is essential for DLBCLs, and MPC inhibition affects glutamine to TCA cycle flux in DLBCL. Related to Figure 2.

(A) Growth assay of OxPhos- and BCR-DLBCL cells cultured in suspension and treated with either vehicle, GLS inhibitor CB-839, or CB-839 with dimethyl-α-ketoglutarate (dmKG). Cell concentration is the mean of n = 3 independent biological experiments, ± standard deviation.

(B) Quantification of the isotopologue abundances of glutamate, citrate, succinate, fumarate, and malate in DLBCL cells cultured with L-[U-^{13}C]-glutamine ± the MPC inhibitor UK-5099 for 30 minutes. Isotopologue abundance is the mean of n = 3 independent biological experiments, ± standard deviation.

(C) Quantification of the isotopologue abundances of glutamate, citrate, succinate, fumarate, and malate in DLBCL cells cultured with L-[U-^{13}C]-glutamine ± the MPC inhibitor UK-5099 for 2 hours. Isotopologue abundance is the mean of n = 3 independent biological experiments, ± standard deviation.

(D) Quantification of the isotopologue abundances of alanine and lactate in the medium collected from DLBCLs grown with D-[U-^{13}C]-glucose ± the MPC inhibitor UK-5099 for 4 hours. Isotopologue abundance is the mean of n = 3 independent biological experiments, ± standard deviation.

Vehicle: Dimethyl sulfoxide (DMSO)

ns $p > 0.05$; *$p < 0.05$; **$p < 0.01$; ***$p < 0.001$; ****$p < 0.0001$. Data were analyzed by one-way Anova followed by Dunnett's multiple comparison test.

Wei et al., Figure S3

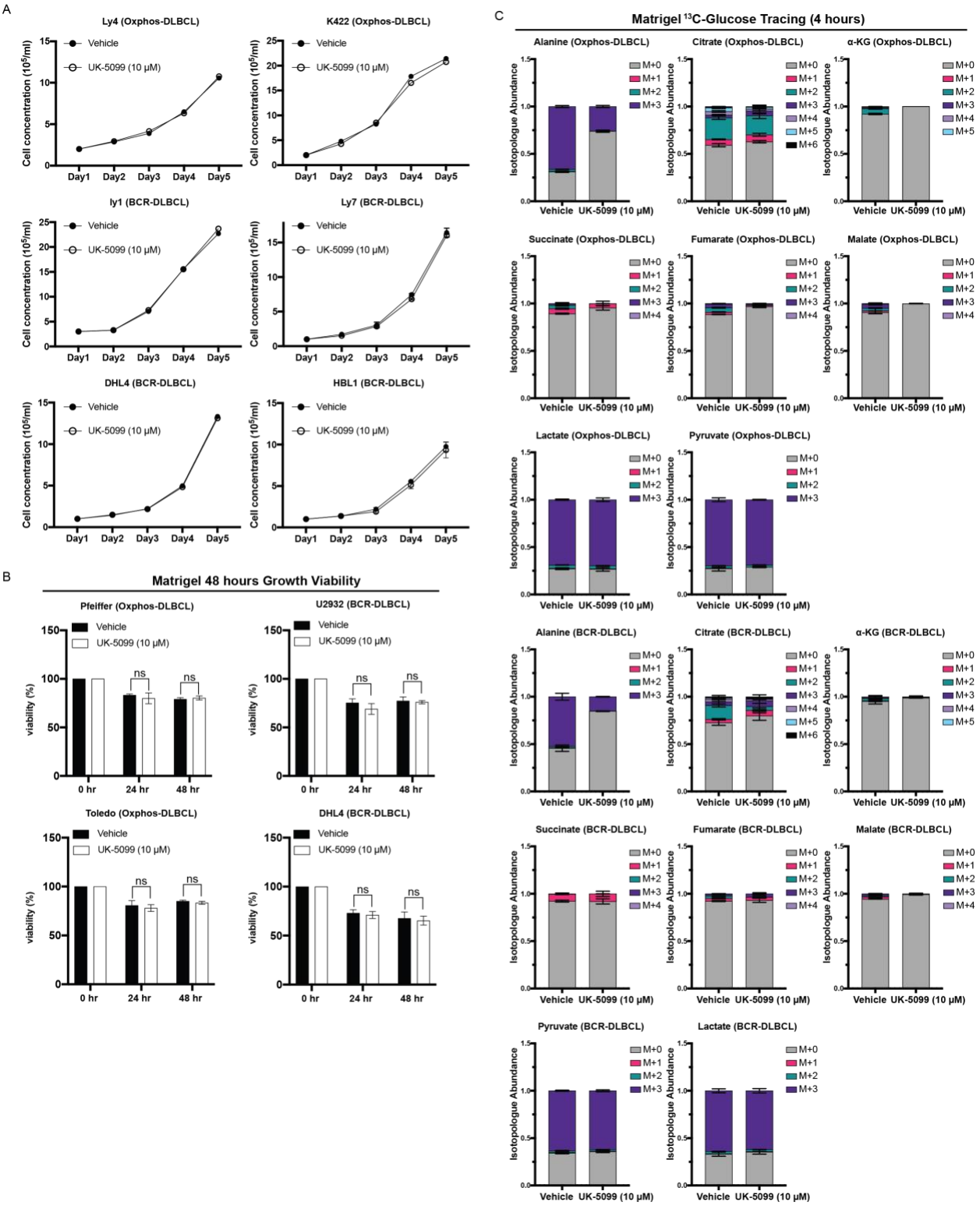

Figure S3. MPC inhibition reduces DLBCL proliferation in Matrigel. Related to Figure 3.

(A) Growth assay of DLBCL cell lines cultured in suspension ± the MPC inhibitor UK-5099 for five days. Cell concentration is the mean of n = 3 independent biological experiments, ± standard deviation.

(B) Cell viability measured by trypan blue staining of DLBCL cell lines cultured in Matrigel ± the MPC inhibitor UK-5099 for 48 hours. Cell viability is the mean of n = 3 independent biological experiments, ± standard deviation.

(C) Quantification of the isotopologue abundances of alanine, citrate, α-KG, succinate, fumarate, malate, lactate, and pyruvate from OxPhos- and BCR-DLBCL cells cultured in Matrigel with D-[U-^{13}C]-glucose ± the MPC inhibitor UK-5099 for 4 hours. Isotopologue abundance is the mean of n = 3 independent biological experiments, ± standard deviation.

Vehicle: Dimethyl sulfoxide (DMSO)

ns p >0.05; *p < 0.05; **p < 0.01; ***p < 0.001; ****p < 0.0001. Data were analyzed by one-way Anova followed by Dunnett's multiple comparison test.

Wei et al., Figure S4

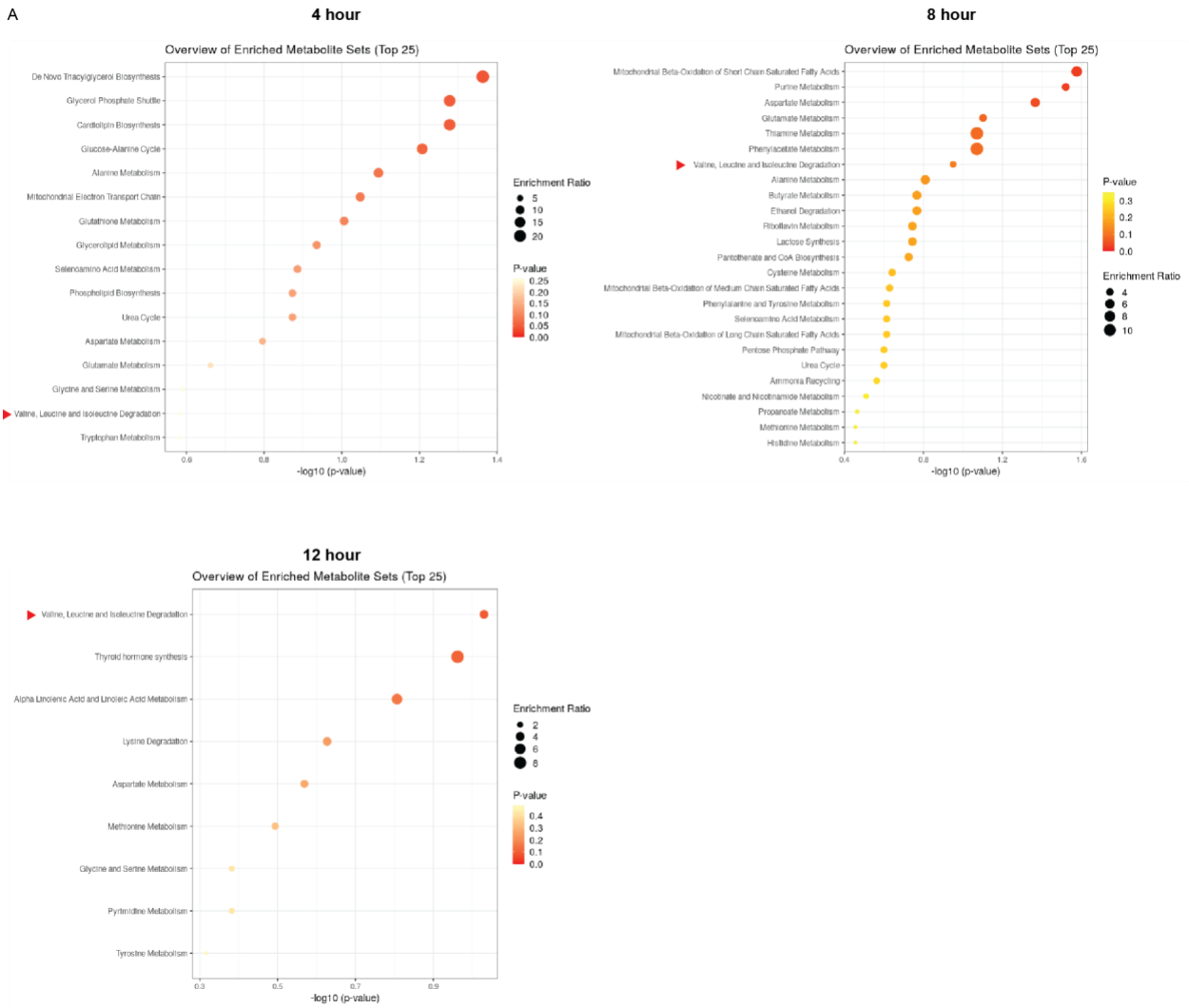

Figure S4. BCAA degradation pathway is affected by MPC inhibition. Related to Figure 6.

(A) Metabolite set enrichment analysis based on MPC inhibition (vehicle vs. UK-5099) of cells grown in Matrigel for 4 hours, 8 hours, and 12 hours. Metabolite abundances are n = 3 independent biological experiments. Arrowheads are pointing to BCAA degradation pathways.

Vehicle: Dimethyl sulfoxide (DMSO)

ns p >0.05; *p < 0.05; **p < 0.01; ***p < 0.001; ****p < 0.0001. Data were analyzed by one-way Anova followed by Dunnett's multiple comparison test.

Wei et al., Figure S5

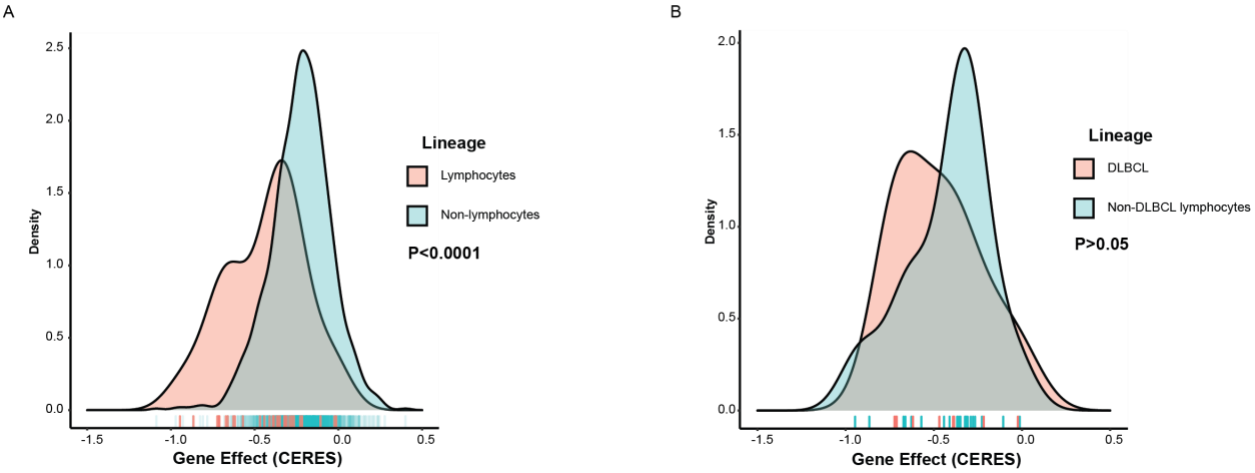

Figure S5. SLC25A1 dependency in cancer cell lines. Related to Figure 7.

(A) Distribution of dependency for SLC25A1 comparing cancer cell lines of the lymphocyte lineage versus cancer cell lines from all other lineages.

(B) Distribution of dependency for SLC25A1 restricted to the lymphocyte lineage, comparing DLBCL versus other subtypes.

Tick marks indicate individual cell lines. Dependency data downloaded from DepMap release 21Q2.